Mitochondrial respiratory-chain adaptations in macrophages contribute to antibacterial host defense

Johan Garaude[1,2,8,9], Rebeca Acín-Pérez[1,8], Sarai Martínez-Cano[1], Michel Enamorado[1], Matteo Ugolini[3], Estanislao Nistal-Villán[4], Sandra Hervás-Stubbs[4,5], Pablo Pelegrín[6], Leif E. Sander[3], José A. Enríquez[1,7,9], & David Sancho[1,9]

[1]Centro Nacional de Investigaciones Cardiovasculares Carlos III (CNIC), Melchor Fernández Almagro, 3, 28029 Madrid, Spain.
[2]Institute for Regenerative Medicine and Biotherapies, Institut National pour la Santé et la Recherche Médicale, U1183, 80 Avenue Augustin Fliche, 34295 Montpellier Cedex 5, France.
[3]Department of Infectious Diseases and Pulmonary Medicine, Charité Hospital Berlin, Augustenburger Platz 1, 13352 Berlin, Germany.
[4]Centro de Investigación Médica Aplicada, Universidad de Navarra, Pio XII, 55 E-31008 Pamplona, Spain.
[5]Instituto de Investigación Sanitaria de Navarra (IDISNA), Recinto de Complejo Hospitalario de Navarra, E-31008, Pamplona, Spain.
[6]Unidad de Inflamación y Cirugía Experimental, Centro de Investigación Biomédica en Red en el Área Temática de Enfermedades Hepáticas y Digestivas, Hospital Clínico Universitario Virgen de la Arrixaca, Instituto Murciano de Investigación Biosanitaria-Arrixaca (IMIB-Arrixaca), 30120 Murcia, Spain.
[7]Departamento de Bioquímica y Biología Molecular y Celular. Universidad de Zaragoza. Zaragoza, Spain.
[8]These authors contributed equally to this work.
[9]These authors jointly supervised this work.
Correspondence and requests for materials should be addressed to J.G. (johan.garaude@inserm.fr), J.A.E (jaenriquez@cnic.es), or D.S (dsancho@cnic.es).

The mitochondrial electron transport chain (ETC) is a metabolic hub whose adaptations accompany fuel source fluctuations, stress responses, and innate

immune signals to ensure optimal cellular functions. Macrophages tightly scale their core metabolism upon activation by innate immune receptors but the precise regulation of the ETC upon pathogen recognition and its functional implications are currently unknown. Here we show that innate immune sensing of live bacteria by macrophages elicits transient ETC adaptations that is characterized by a decrease assembly of complex I (CI) and CI-containing supercomplexes and by a switch in the relative contribution of complexes I and II to mitochondrial respiration. This is mediated by the phagosomal nicotinamide adenine dinucleotide phosphate (NADPH)-oxidase and the reactive oxygen species (ROS)-dependent Src-family tyrosine-kinase Fgr and required Toll-like receptor (TLR) signalling and the NOD-like receptor (NLR) family, pyrin domain–containing protein 3 (NLRP3) inflammasome, both connected to bacterial viability-specific immune responses Consistently, the inhibition of CII in *E. coli* infected mice decreases IL-1β and increases IL-10 serum-levels to those found in mice treated with dead bacteria and impairs control of bacteria. We thus identify the innate immune receptor-mediated ETC adaptations as an early immune-metabolic checkpoint that potentially adjusts innate immune responses during bacterial infection.

Macrophages are phagocytic immune cells that reside in most tissues thereby constituting the first line of host-defence to invading microorganisms and tissue damage[1]. They express a wide variety of innate immune receptors allowing them to tightly determine the nature of the threats and to finely tune their differentiation program towards the most appropriate to eliminate those threats or to engage tissue repair processes[2]. Indeed, the combinatory detection by macrophages of microbial features such as pathogenicity viability and invasiveness scales the nature and the strength of the immune response generated[3]. Recent studies demonstrate that adaptations of cellular metabolism are critically associated to macrophage activation[4, 5, 6, 7] and accumulating evidence indicates that such adaptations indeed contribute to macrophage functions[8]. As other cell types, macrophages are able to metabolize a variety of carbon substrates, including glucose, fatty acids, ketone bodies and amino acids. The choice of cellular fuel is not only dictated by the availability of a specific fuel but also by particular biosynthetic needs or

engagement of pathogen recognition receptors (PRRs) and cytokine receptors thereby enabling adaptations to infection, stress and differentiation requirements[8, 9, 10].

Activation of macrophage through the Toll-like receptor 4 (TLR4) using Gram-negative bacterial cell wall lipolysaccharide (LPS) induces profound metabolic reprogramming that culminates in enhanced glycolysis and lactate production while glutamine replenishes the tricarboxylic acid (TCA) cycle through glutaminolysis[5, 7]. Accumulation of the TCA intermediate succinate in LPS-stimulated macrophages together with increased reactive oxygen species (ROS) level stabilize hypoxia inducible factor 1α (HIF-1α), which in turn regulates the transcription of the pro-form of interleukin (IL)-1β[7]. In addition, TLR4 engagement promotes glycolysis[6] and regulates the glycolytic enzyme hexokinase 1 that activates the pyrin domain–containing protein 3 (NLRP3) inflammasome to promote pro-IL-1β processing[11]. Accumulation of TCA cycle intermediates may also directly contribute to macrophage antimicrobial functions. For example, LPS-activated macrophages accumulate citrate that can be converted into cis-aconitate, which is in turn metabolized in itaconic acid, the enzymatic product of the protein encoded by *immune responsive gene 1* (*Irg1*)[5, 12]. This metabolite was found to have direct antibacterial properties on various pathogens including *Salmonella enterica* Typhimurium, *Mycobacterium tuberculosis* or *Legionella pneumophila* [12, 13]. Those are few examples of how metabolic reprogramming is contributing to macrophage-mediated inflammation. Interestingly, such proximity between cellular metabolism and inflammatory events was also evident in sepsis patient whose monocytes exhibit distinct metabolic signatures when isolated during the acute phase of the disease or during the resolution phase[14].

At the core of the metabolic pathways is the mitochondrion, a bioenergetic organelle that not only contributes to energy supply, bionsynthesis or cellular redox maintenance, but also serves as a signalling platform for various innate immune signalling pathways[9, 10, 15]. Mitochondria balance their contribution to anabolism and catabolism in response to fuel or oxygen availability and extracellular signals including danger signals and cytokines[8, 9]. All fuel catabolic processes converge on the mitochondrial electron transport chain (ETC) by supplying electrons in the form of the reductive equivalents nicotinamide adenine dinucleotide (NADH) and flavin adenine

dinucleotide ($FADH_2$). The ETC comprises two electron carriers (coenzyme Q [CoQ]/ubiquinone and cytochrome c) and four respiratory complexes (complex I to IV [CI to CIV]), which, except for CII, can dynamically assemble as larger molecular supercomplexes (SCs) in the mitochondrial inner membrane[16, 17]. The dynamic assembly of respiratory complexes into SCs have been proposed to confer functional advantages to the cells, which includes potentiating electron flux within the ETC, preventing the generation of ROS by sequestering reactive intermediates or stabilizing individual respiratory complexes[16]. Whether super assembly of ETC respiratory complexes can contribute to immune function remains to be determined. Nevertheless, several recent studies highlighted the potential importance for ETC respiratory complexes in macrophage activation. Chemical inhibition of CI impairs the production of the pro-inflammatory cytokine interleukin (IL)-1β while induces secretion of the anti-inflammatory IL-10 in activated macrophage[18]. In contrast, the genetic ablation of the CI subunit NDUFS4 enhances macrophage inflammatory phenotype[19] suggesting that CI activity rather dampens macrophage activation.

Here, we hypothesized that adaptations of the ETC would indeed contribute to the metabolic switch undergone by myeloid cells upon activation via innate immune receptors[5, 7]. We report that innate immune sensing of viable Gram-negative bacteria through TLR and NLRP3 induces a phagosomal ROS-dependent transient decreased abundance of supercomplexes within the macrophage mitochondria due to destabilization of CI. The resulting decrease in CI activity is inversely reflected by an increase in the activity of the FAD-dependent enzymes CII, which contributes to antimicrobial function. Inhibition of CII during viable bacteria detection by macrophage modulates levels of IL-1β and IL-10 to those found upon dead bacteria encounter, suggesting that manipulation of ETC components may be offer therapeutically interest.

RESULTS

Sensing of bacteria provokes changes in mitochondrial ETC architecture. To determine whether innate immune cell activation impacts the respiratory chain, we first analysed the ETC organization of mouse *CD1* bone-marrow-derived macrophages (BMDMs) challenged or not with viable *Escherichia coli* K12, strain DH5α (*E. coli*) for

1.5h. Two-dimensional gel analysis of mitochondria isolated from BMDMs revealed several respiratory SCs including the respirasome (SC I+III_2+IV), SC I+III_2 and SC III_2+IV[20, 21] in both resting and stimulated macrophages (Fig. 1a and Supplementary Fig. 1a). We then examined a potential SC alteration and performed blue-native (BN)-PAGE analysis of whole cell, which revealed a decrease in CI and CI-containing SC (the respirasome and SC I+III_2) abundance when *CD1* macrophages sensed live *E. coli* (Fig. 1b, right panel). Protein levels of various ETC subunits were unaffected by *E. coli* challenge, despite mild transcriptional variations of some ETC-subunit-encoding nuclear genes (Supplementary Fig. 1b-f), indicating alteration of SC assembly rather than changes in protein expression. Importantly, macrophages from *C57BL/6* mice, which unlike *CD1* mice lack the long isoform of supercomplex assembly factor I (SCAFI, Cox7a2l) and consequently do not assemble CIV-containing SCs[21], exhibited a transient reduction in the amounts of CI and CIII engaged in SCs (Fig. 1b-e and Supplementary Fig. 2a and 2b). Therefore the disassembly of CI and CI-containing SCs upon detection of viable bacteria is not restricted to those containing CIV. Bacteria-induced ETC alteration was also evident in mouse *C57BL/6* peritoneal macrophages (Supplementary Fig. 2c), and was not limited to *E. coli* detection, as shown by the diminished abundance of CI and SC I+III_2 upon recognition of *Salmonella enterica* serovar Typhimurium SL1344 (*S. enterica* Typhimurium) (Supplementary Fig. 2d-f).

Detection of bacteria modulates ETC complex activities. Macrophages activated through innate immune receptors use fatty acids and glutamine rather than glucose as the carbon source for oxidative phosphorylation[5, 7]. This adaptation results in a shift in the proportion of NADH/$FADH_2$ electrons feeding the ETC[22], which may require the modulation of relative SC proportions[21]. Indeed, stimulation of BMDMs by *E. coli* or *S. enterica* Typhimurium, transiently decreased the in-gel respiratory activities of CI within the respirasome (SC I+III_2+IV) and SC I+III_2 (Fig. 1b, 1d and Supplementary Fig. 2f) reflecting the decreased CI abundance within SCs. Quantitative spectrophotometric assessment of CI and CI+CIII activities in isolated mitochondria confirmed the decrease in CI-mediated respiration in response to *E. coli* while total CIII and CIV activities remained unaltered and CII was increased as explained below (Fig. 2a). To determine

whether the decreased CI activity translated into a drop in energy production, we measured mitochondrial-ATP production rate in permeabilized BMDMs in the presence of glutamate plus malate, which generate intramitochondrial NADH that feeds electrons to CI[21]. We thereby found that CI-dependent ATP production was diminished upon *E. coli* sensing (Fig. 2b). Thus, macrophage activation was characterized by decreased CI assembly into SCs and decreased overall CI activity, consistent with an anti-inflammatory role of CI in macrophages[19]. In line with the effect of the bacterial cell-wall component lipopolysaccharide (LPS) stimulation in macrophages[4, 5, 7], BMDMs treated with *E. coli* markedly lowered their O_2 consumption on glucose substrate, while exerting a high glycolytic activity that increased the extracellular acidification rate (ECAR) and lactate production at 18h post-infection (Supplementary Fig. 3a-c). However, we found that the maximal respiration rate (MRR) was increased in *E. coli*-treated BMDMs at 1.5h post-challenge (Fig. 2c and Supplementary Fig. 3d), creating a situation in which spare respiratory capacity (SRC) (Fig. 2d), ECAR (Fig. 2e) and lactate production (Fig. 2f) were increased simultaneously.

Sensing of *E.coli* stimulates mitochondrial CII and glycerol-3-phosphate dehydrogenase. The concomitant reduction in CI+CIII activity and the increased MRR of *E. coli*-stimulated macrophages on glucose substrate appears contradictory and suggested that an alternative electron source would compensate the expected reduction in NADH (CI)-dependent electron flux. We hypothesized that the *E. coli*-infection-driven alteration of macrophage ETC and the resulting decrease in CI activity would favour the use of electrons coming from the $FADH_2$-oxidizing enzymes, as shown previously[16, 21, 23]. We indeed found a robust increase in CII and CII+CIII activities in mitochondria isolated from *E. coli*-stimulated macrophages (Fig. 2a). Similarly, CII enzymatic activity was augmented peritoneal *C57BL/6* macrophages (Fig. 3a), human $CD14^+CD16^-$ monocytes (Fig. 3b), and BMDMs challenged with *S. enterica* Typhimurium (Fig. 3c). Macrophage detection of *E. coli* increased the CII-mediated ATP production rate (Fig. 3d) as opposed to CI (Fig. 2b) suggesting a switch in the individual contribution of those complexes to energy production in this setting. The increased activities of CII (Fig. 3e) and CII+III (Fig. 3f) were transient, reflecting the dynamics in SC reorganization (Fig. 1d and 1e). The use

of glucose catabolism to increase the maximum respiration rate despite a decrease in CI function (Fig. 2a-d) would necessitate the delivery of NADH electrons generated by glycolysis to the mitochondrial electron transport chain without the utilization of CI. This can be achieved by shuttling cytoplasmic NADH electrons to CoQ by mitochondrial bound glycerol-3-phosphate dehydrogenase (mG3PDH)[24]. Similar to CII, mG3PDH (Fig. 3g and 3h) and mG3PDH+CIII (Fig. 3i) activities were increased. Nevertheless, the kinetics were different since CII activity reached its maximum at 0.5h to 1.5h after EC challenge, whereas the induction of mG3PDH was maintained for longer. Taken together, these data indicate that *E. coli* recognition induces a transient reorganization of SCs in macrophages, which could make CIII available for electrons provided by $FADH_2$ dependent enzymes and thereby allowing mitochondria to re-oxidize cytoplasmic NADH without the use of CI[16, 21].

The phagosomal NADPH oxidase and the Src-family kinase Fgr are required for ETC adaptations. Mitochondrial ROS (mROS), which increased within a few hours upon *E. coli* sensing[25], are inherent to ETC function making them potential regulators of CII activity in *E. coli*-stimulated macrophages. However, we were unable to detect substantial mROS production enhancement 1.5h after *E. coli* challenge (Supplementary Fig. 4a and 4b). We nevertheless found that both the mROS-specific inhibitor mitoQ[26] and the broad antioxidant N-acetyl cysteine (NAC) prevented basal and *E. coli*-induced CII activity in macrophages (Fig. 4a). Those data suggested that mROS are required for proper CII functions in macrophages but impelled us to investigate an alternative potent source of ROS induced upon *E. coli* sensing that would trigger CII activity. Another important source of ROS in macrophages is the phagosomal nicotinamide adenine dinucleotide phosphate (NADPH)-oxidase[27]. A 15min challenge with *E. coli* strongly thus induced ROS production that was entirely dependent on the expression of the NADPH oxidase subunit $gp91^{PHOX}$ (Supplementary Fig. 4c-e). Strikingly, *gp91phox*$^{-/-}$ macrophages were not able to induce CII activity in response to *E. coli* (Fig. 4b). *E. coli*-mediated increase in SRC was absent in *gp91phox*$^{-/-}$ BMDMs (Fig. 4c and Supplementary Fig. 4f and 4g) while ECAR induction was unaffected (Fig. 4d). The absence of $gp91^{PHOX}$ also prevented *E. coli*-induced SC rearrangement in isolated mitochondria (Fig.

4e and 4f). Taken together, our data identify phagosomal ROS as early inducers of ETC adaptations during bacterial sensing that would cooperate with mROS to complete those adaptations.

CII activity adapts to fuel use through H_2O_2-mediated activation via SDHA subunit phosphorylation by the Src-family tyrosine kinase Fgr (Gardner-Rasheed feline sarcoma virus homolog)[28], the partner kinase of the phosphatase PTPMT1 (Protein Tyrosine Phosphatase, Mitochondrial 1)[29]. We indeed found that the absence of Fgr prevented *E. coli*-induced regulation of CI and CII activities and prevented SC rearrangement in permeabilized BMDMs (Fig. 4g and Supplementary Fig. 5a-e) or isolated mitochondria (Supplementary Fig. 5f-j). *Fgr*$^{-/-}$ BMDMs were unable enhance CII-mediated ATP production and had a preserved CI-dependent ATP production (Fig. 4h) upon *E. coli* detection. As a consequence, Fgr deficiency in BMDMs prevented the increase in MRR (Supplementary Fig. 5k) and SRC (Fig. 4i) but did not affect the increase in ECAR (Fig. 4j) or lactate production (Fig. 4k) upon *E. coli* challenge. These results identify Fgr as an important regulator of macrophage ETC adaptations during bacterial infection.

Metabolic reprogramming towards glycolysis and accumulation of succinate[7], together with an increase in mitochondrial ROS production[25], all contribute to antimicrobial functions of macrophages. In line with this, *Fgr*$^{-/-}$ BMDMs showed increased intracellular bacteria upon infection *in vitro*, indicating enhanced survival of *E. coli* within BMDMs (Fig. 4l). However, Fgr-deficiency was not sufficient to increase intraperitoneal *E. coli* infection (Supplementary Fig. 5l and 5m). *E. coli* stimulation of *Fgr*$^{-/-}$ BMDMs did not affect the induction of the inflammatory genes *Il1b*, *Ifnb* and *Tnf* (Supplementary Fig. 5n) despite a slight decrease in IL-1β production (Supplementary Fig. 5o). These data likely reflect a compensatory action of other Src-family kinases for inflammatory cytokine expression[30].

CII activity contributes to anti-microbial responses. Since Fgr has other targets besides CII, we decided to block CII activity with the SDH-specific inhibitor 3-nitropropionic acid (NPA)[31] in order to determine the exact contribution of the early pathogen-driven CII activation to mitochondrial respiration and macrophage immune function. At the concentrations tested, NPA did not affect BMDM survival or phagocytic

activity (Supplementary Fig. 6a and 6b), but strongly repressed CII activity in resting and *E. coli*-stimulated BMDMs (Supplementary Fig. 6c) without affecting bacterial SDH activity or growth (Supplementary Fig. 6d and 6e). Treatment of BMDMs with NPA did not prevent SC disassembly (Supplementary Fig. 6f) or the drop in CI-mediated ATP production, but efficiently prevented CII-mediated ATP production induced by *E. coli* challenge (Supplementary Fig. 6g). We then found that NPA treatment strongly reduced the MRR induced by *E. coli* (Fig. 5a and Supplementary Fig. 6h) and ablated the SRC (Fig. 5b) without affecting ECAR induction (Fig. 5c and Supplementary Fig. 6i) or lactate production (Supplementary Fig. 6j). Similar results were obtained using the CII competitive inhibitor dimethyl-malonate (DM)[32] or thenoyltrifluoroacetone (TTFA) (Supplementary Fig. 6k-p). We next investigated whether CII activity contributed to macrophage anti-microbial function. Mice treated with NPA were more susceptible to *S. enterica* Typhimurium infection (Fig. 5d), and presented an increased splenic bacterial burden at 72h after intra-peritoneal infection with viable *E. coli* (Fig. 5e) despite normal recruitment of inflammatory cells to the peritoneal cavity (Supplementary Fig. 7a). This higher bacterial load (Fig. 5e) was associated with decreased serum levels of the pro-inflammatory cytokine IL-1β and increased levels of anti-inflammatory cytokine IL-10, while TNFα levels were not affected (Fig 5f). Similar to our data obtained with *Fgr*$^{-/-}$ BMDMs (Fig. 4i), NPA treatment impaired BMDMs bactericidal activity *in vitro* (Fig. 5g and 5h). In addition, NPA-treated BMDMs showed reduced levels of *E. coli*-induced IL-1β protein and *Il1b* and *Ifnb* mRNA, but not TNFα (Supplementary Fig. 7b and 7c), consistent with the relative insensitivity of TNFα production to macrophage-metabolic fluctuations and oxygen availability[7, 33]. Itaconic acid, which results from decarboxylation of the tricarboxylic acid (TCA) cycle intermediate *cis*-aconitate, was recently shown to have anti-bacterial properties[12]. Similarly, we found that the TCA cycle intermediate fumarate, which is produced by the oxidation of succinate by CII, strongly inhibited bacterial growth (Supplementary Fig. 7d) and induced bacterial death (Supplementary Fig. 7e and 7f) while succinate had negligible effect. To exclude that merely lowering the pH accounted for the observed effects of fumarate on bacteria viability, we used ester forms of these TCA intermediates. Dimethyl-fumarate but not dimethyl-succinate impaired *E. coli* and *S. enterica* Typhimurium growth (Fig. 5i and Fig.

5j, respectively). These data identified CII as an important contributor to the macrophage mitochondrial respiratory functions needed for anti-microbial responses.

Innate immune receptor-mediated detection of microbial viability triggers ETC adaptations. The highly specific metabolic response to bacteria was not observed when heat-killed *E. coli* or LPS were used to stimulate macrophages (Supplementary Fig. 8a-b, 5h, 5j). This prompted us to investigate the nature of the bacterial stimuli that trigger ETC adaptations. In contrast to viable *E. coli*, heat-killed *E. coli* challenge did not affect the assembly of the respirasome and CI-containing SCs (Fig. 6a and Supplementary Fig. 8a-b). Moreover, heat-killed *E. coli* did not impair CI in-gel activity within $I+III_2$ SC (Fig. 6a lower panel) or CI+CIII activity measured in mitochondria (Supplementary Fig. 5j), and failed to increase mitochondrial MRR (Supplementary Fig. 8c) or SRC (Fig. 5b). However, viable and heat-killed *E. coli* both efficiently induced ECAR (Fig. 5c), lactate release (Supplementary Fig. 8d) and mG3PDH activity (Supplementary Fig. 8e) likely reflecting the capacity of LPS to trigger a glycolytic switch in macrophages[5, 7]. In contrast, heat-killed *E. coli* were unable to induce CII activity in BMDMs (Fig. 5d), human $CD14^+CD16^-$ monocytes (Fig. 5e) or peritoneal macrophages (Supplementary Fig. 8f). Importantly, live *E. coli* were more efficient than heat-killed *E. coli* at inducing phagosomal ROS production (Fig. 5f and Supplementary Fig. 8g), which is required for CII and SRC induction in macrophages (Fig. 4b and 4c). These findings indicate that stimuli associated with viable bacteria trigger ETC adaptations in macrophages.

An association with viability has been suggested for several bacterial molecules[3, 34], including bacterial messenger RNAs[35]. Indeed we found that CII activity was enhanced in response to RNA purified from *E. coli* and unaffected when the RNA preparations were pre-treated with RNases (Fig. 4g and Supplementary Fig. 8h). The double-stranded RNA-mimicking polyinosinic:polycytidylic acid (poly(I:C)) and the single-stranded RNA-mimicking R848 – which respectively trigger the Toll-like receptor 3 (TLR3) and TLR7 – also induced CII activity, whereas the TLR4 agonist LPS or the DNA-mimicking TLR9 agonist CpG oligodeoxynucleotide did not (Fig. 6h and Supplementary Fig. 8i-j). This was also evident in human $CD14^+CD16^-$ monocytes (Fig. 5e). In addition, poly(I:C) treatment decreased CI-mediated ATP production and

promoted CII-mediated ATP production in permeabilized BMDMs (Fig. 5i). These results indicated that recognition of microbial RNA controls CII activity. Since bacterial mRNA triggers viability-specific immune responses through TIR-domain-containing adapter-inducing interferon-β (TRIF)[35], we evaluated the contribution TLR adaptors to ETC changes induced by *E. coli*. We found that BMDMs singly or doubly deficient for TRIF and myeloid differentiation primary response 88 (MyD88) were unable to induce CII activity when exposed to bacteria (Fig. 5j). In contrast, induction of CII activity upon *E. coli* challenge was unaffected in BMDMs deficient for stimulator of interferon genes (STING) or interferon-β promoter stimulator (IPS-1, also known as mitochondrial antiviral signalling or MAVS), two adaptors that use mitochondria to mediate nucleic acids and poly(I:C) sensing by cytosolic receptors[15] (Supplementary Fig. 8k). In addition, both TRIF and MyD88 were required to initiate changes in ETC composition upon EC sensing (Fig. 5k, 5l and Supplementary Fig. 8l). Thus, adjustments of the CII function in response to bacteria are likely regulated by phagosomal RNA-sensing TLRs rather than cytosolic nucleic acid-sensing innate immune receptors[3]. Viability-specific immune responses and bacteria RNA sensing also involve the NOD-like receptor (NLR) family, pyrin domain–containing protein 3 (NLRP3) inflammasome[3, 35, 36], the activation of which has previously been linked to mitochondria, phagosomal NADPH oxidase and ROS release[3, 15, 35, 36, 37]. Both CII induction (Fig. 5m) and ETC rearrangement (Fig. 5n and Supplementary Fig. 8m) were remarkably impaired in BMDMs deficient for NLRP3 or for the inflammasome effector caspases caspase1 and caspase11 thereby placing CII activation in the centre of viability-specific immune responses to bacteria. Consistently, treatment of *E. coli*-infected *Wt* mice with the CII inhibitor dimethyl-malonate decreased serum levels of IL-1β and increased serum levels of IL-10 to levels measured in heat-killed *E. coli*-treated mice without influencing IL-6 levels (Fig. 7).

DISCUSSION

Our study unravels a mechanism by which macrophages adjust their metabolism in response to viable bacteria by coupling TLR engagement, the NLRP3 inflammasome and ROS signalling to mitochondrial electron transport chain. This metabolic adjustment

in turn contributes to the initiation and scaling of pathogen-specific immune responses (Fig. 8).

We found that ETC architecture is altered in response to viable bacteria detection because of a decrease in the abundance of assembled CI. Several explanations can account for this. CI is an unstable ETC multiprotein complex composed of 44 different protein subunits, the assembly of which is influenced by the oxidative environment within the ETC[16] and/or by previous assembly of other ETC components including CIII[38] or cytochrome c[39]. It was recently demonstrated that a switch in substrate that fuels the TCA cycle modifies the NADH to $FADH_2$ ratio, which can saturate the oxidation capacity of the CoQ pool thereby inducing a reverse electron transfer (RET) towards CI. This in turn increases superoxides that oxidize specific CI proteins thereby leading to disassembly of the complex[40]. Upon surface TLR engagement ROS levels within the ETC is increased[25], and thus constitute a potential source of CI-destabilizing ROS. In addition, a RET-inducing modulation of the NADH/$FADH_2$ ratio is likely to occur here since innate immune receptor activation diverts pyruvate from entering the mitochondria and decrease fatty acid oxidation while glutaminolysis ensures the replenishment of the TCA cycle[5, 41]. However, unless a yet to be determined bacteria viability-specific metabolic flux adaptation further modulates the NADH/$FADH_2$ ratio, CI destabilization should equally occur in response to both heat-killed and viable bacteria but we only observed ETC alterations in response to the later. In addition, the inhibition of CII in macrophage challenged with viable *E. coli* did not impair the decrease in CI and CI-containing SC abundance nor it prevented the decrease in CI-mediated ATP synthesis. Phagosomal ROS may also account for the oxidative destabilization of CI. Indeed, we found that $gp91^{PHOX}$-deficient macrophage had preserved ETC architecture in response to viable *E. coli*. However, $pg91^{PHOX}$ deficiency also impaired CII activity induction, and as a consequence could also prevent CI-destabilizing RET. Therefore, whether changes in ETC architecture upon viable bacterial challenge are a consequence of the rapid increase an oxidative burst within the ETC due innate immune signalling or result from fuel switch remains to be determined.

Whether metabolic reprogramming directly contributes to macrophage effector function is an important question that recently emerged. It has been demonstrated that

itaconate, a nonamino organic acid, can exert antimicrobial functions in concentration range about 10mM[12, 13]. Consistent with this notion, we found that CII-enzymatic product fumarate, but not its precursor succinate, prevented bacteria growth *in vitro* and decreased bacterial viability at a concentration of 10mM. At such concentration pH is merely decreased and should therefore impair macrophage normal functions. However, upon bacteria encounter by macrophages, mitochondria are juxtaposed to microbe-containing phagosomes[25, 42]. This is mediated by the formation of a complex between the TLR signalling adaptor TNF receptor-associated factor 6 (TRAF6) and the mitochondrial complex I-assembly factor ECSIT[25], the interaction of which is regulated by a Mst1-Mst2-Rac signalling axis[42]. Such proximity between mitochondria and bacteria-containing phagosomes might permit the delivery of mROS or mitochondrial metabolites to contribute to bacteria killing[15]. Such model presents some advantages since it would allow reaching sufficient concentration of those 'antimicrobial metabolites' locally (i.e. within the phagosome) while sparing host cellular metabolism. Future work will likely provide additional insights on this issue.

The use of LPS to activate macrophage generated a considerable amount of information on the metabolic pathways and reprogramming engaged during inflammation [8]. We found that challenge of macrophage with heat-killed bacteria indeed recapitulates many aspects of LPS-mediated TLR4 engagement on mitochondrial respiration including induction of glycolytic flux (increased ECAR and lactate release) and decreased oxygen consumption in the mitochondria. However, the induction of CII activity and destabilization of the ETC was observed only in response viable bacteria. Therefore, while the use of a single pathogen-associated molecular pattern (PAMP) certainly present advantages, it only offers a partial view of the complexity of the innate immune signals that may regulate metabolic adjustments upon the encounter of a whole viable microorganism. This is not trivial since macrophages tightly scale their response to many features of bacteria including viability-specific signals[3, 34]. Most importantly, we found that the inhibition of CII during viable bacteria challenge in mice increased IL-10 and decreased Il-1β serum levels to those observed when heat-killed bacteria were used. Thus, the establishment of a functional link between pattern recognition receptors, ETC organization and subsequent inflammatory immune responses may offer substantial

benefits for vaccine design and provide valuable new targets for pharmacological intervention both during infection and in metabolic inflammatory disorders.

METHODS

Methods and any associated references are available in the online version of the paper.

Note: Any Supplementary Information is available in the online version of the paper.

ACKNOWLEDGMENTS

We are grateful to A. Hidalgo for critical reading of the manuscript, J. Magarian Blander for *Myd88*$^{-/-}$, *Trif*$^{/-}$ and *Trif*$^{/-}$*Myd88*$^{-/-}$ mice, F. Norel-Bozouklian for *Salmonella thyphimurium* SL1344, S. Trombetta for the plasmid encoding GFP-OT and S. Bartlett for English editing. We thank M. Fernández-Monreal, M. Villalba, F. Ruperez-Pascualena and Sancho and Enríquez lab members for insightful discussions and support. J.G. holds a 'Juan de la Cierva' fellowship and R.A.-P. holds a Ramon y Cajal fellowship, both from the Spanish Ministry of Economy and Competitiveness. This work was funded by a European FP7-Marie Curie Career Integration Grant #332881 and a grant from the French association 'La Ligue Contre le Cancer-comité du Gard' (CG/59-2013) to J.G., by the CNIC and grants from the Spanish Ministry of Economy and Competitiveness (SAF-2013-42920R to DS; SAF2012-1207 to JAE), the European grants ERC-2010-StG 260414, 635122-PROCROP H2020, to DS and UE0/MCA1108 and UE0/MCA1201 to JAE, the Comunidad de Madrid (CAM/API1009 to JAE). L.E.S. is supported by the German research council (DFG grant SA1940/2-1 and SFB-TR84 TP-C08). The CNIC is supported by the Spanish Ministry of Economy and Competitiveness and the Pro-CNIC Foundation.

AUTHOR CONTRIBUTIONS

J.G and R.A.-P. designed and performed all experiments. S.M.-C. and M.E. performed experiments measuring OXPHOS enzymatic activities, prepared samples for BN-PAGE and western blot and helped with experiments in mice. M.U. and L.E.S. performed experiments with human monocytes. E.N.-V. and S.H.-S. provided bone marrow

progenitor cells from *GT-Sting* and *Ips-1*$^{-/-}$ mice and generated *Ips1*$^{-/-}$*Trif*$^{-/-}$ mice. P.P. provided *Nlrp3*$^{-/-}$ and *Casp1*$^{-/-}$*Casp11*$^{-/-}$ mice. J.G, R.A.-P., J.A.E. and D.S directed the study, analysed the data and wrote the manuscript.

COMPETITING FINANCIAL INTERESTS

The authors declare no competing financial interests

REFERENCES

1. Ginhoux F, Jung S. Monocytes and macrophages: developmental pathways and tissue homeostasis. *Nat Rev Immunol* 2014, **14**(6)**:** 392-404.

2. Taylor PR, Martinez-Pomares L, Stacey M, Lin HH, Brown GD, Gordon S. Macrophage receptors and immune recognition. *Annual review of immunology* 2005, **23:** 901-944.

3. Blander JM, Sander LE. Beyond pattern recognition: five immune checkpoints for scaling the microbial threat. *Nat Rev Immunol* 2012, **12**(3)**:** 215-225.

4. Huang SC, Everts B, Ivanova Y, O'Sullivan D, Nascimento M, Smith AM*, et al.* Cell-intrinsic lysosomal lipolysis is essential for alternative activation of macrophages. *Nature immunology* 2014, **15**(9)**:** 846-855.

5. Jha AK, Huang SC, Sergushichev A, Lampropoulou V, Ivanova Y, Loginicheva E*, et al.* Network Integration of Parallel Metabolic and Transcriptional Data Reveals Metabolic Modules that Regulate Macrophage Polarization. *Immunity* 2015, **42**(3)**:** 419-430.

6. Rodriguez-Prados JC, Traves PG, Cuenca J, Rico D, Aragones J, Martin-Sanz P, *et al.* Substrate fate in activated macrophages: a comparison between innate, classic, and alternative activation. *J Immunol* 2010, **185**(1)**:** 605-614.

7. Tannahill GM, Curtis AM, Adamik J, Palsson-McDermott EM, McGettrick AF, Goel G*, et al.* Succinate is an inflammatory signal that induces IL-1beta through HIF-1alpha. *Nature* 2013, **496**(7444)**:** 238-242.

8. O'Neill LA, Pearce EJ. Immunometabolism governs dendritic cell and macrophage function. *The Journal of experimental medicine* 2016, **213**(1)**:** 15-23.

9. Stanley IA, Ribeiro SM, Gimenez-Cassina A, Norberg E, Danial NN. Changing appetites: the adaptive advantages of fuel choice. *Trends Cell Biol* 2014, **24**(2)**:** 118-127.

10. Weinberg SE, Sena LA, Chandel NS. Mitochondria in the regulation of innate and adaptive immunity. *Immunity* 2015, **42**(3)**:** 406-417.

11. Moon JS, Hisata S, Park MA, DeNicola GM, Ryter SW, Nakahira K*, et al.* mTORC1-Induced HK1-Dependent Glycolysis Regulates NLRP3 Inflammasome Activation. *Cell reports* 2015, **12**(1)**:** 102-115.

12. Michelucci A, Cordes T, Ghelfi J, Pailot A, Reiling N, Goldmann O*, et al.* Immune-responsive gene 1 protein links metabolism to immunity by catalyzing itaconic acid production. *Proceedings of the National Academy of Sciences of the United States of America* 2013, **110**(19)**:** 7820-7825.

13. Naujoks J, Tabeling C, Dill BD, Hoffmann C, Brown AS, Kunze M*, et al.* IFNs Modify the Proteome of Legionella-Containing Vacuoles and Restrict Infection Via IRG1-Derived Itaconic Acid. *PLoS Pathog* 2016, **12**(2)**:** e1005408.

14. Shalova IN, Lim JY, Chittezhath M, Zinkernagel AS, Beasley F, Hernandez-Jimenez E*, et al.* Human monocytes undergo functional re-programming during sepsis mediated by hypoxia-inducible factor-1alpha. *Immunity* 2015, **42**(3)**:** 484-498.

15. West AP, Shadel GS, Ghosh S. Mitochondria in innate immune responses. *Nat Rev Immunol* 2011, **11**(6)**:** 389-402.

16. Enriquez JA. Supramolecular Organization of Respiratory Complexes. *Annu Rev Physiol* 2016, **78:** 533-561.

17. Schagger H, Pfeiffer K. Supercomplexes in the respiratory chains of yeast and mammalian mitochondria. *The EMBO journal* 2000, **19**(8)**:** 1777-1783.

18. Kelly B, Tannahill GM, Murphy MP, O'Neill LA. Metformin Inhibits the Production of Reactive Oxygen Species from NADH:Ubiquinone Oxidoreductase to Limit Induction of Interleukin-1beta (IL-1beta) and Boosts Interleukin-10 (IL-10) in Lipopolysaccharide (LPS)-activated Macrophages. *The Journal of biological chemistry* 2015, **290**(33)**:** 20348-20359.

19. Jin Z, Wei W, Yang M, Du Y, Wan Y. Mitochondrial complex I activity suppresses inflammation and enhances bone resorption by shifting macrophage-osteoclast polarization. *Cell metabolism* 2014, **20**(3)**:** 483-498.

20. Acin-Perez R, Fernandez-Silva P, Peleato ML, Perez-Martos A, Enriquez JA. Respiratory active mitochondrial supercomplexes. *Mol Cell* 2008, **32**(4)**:** 529-539.

21. Lapuente-Brun E, Moreno-Loshuertos R, Acin-Perez R, Latorre-Pellicer A, Colas C, Balsa E*, et al.* Supercomplex assembly determines electron flux in the mitochondrial electron transport chain. *Science* 2013, **340**(6140)**:** 1567-1570.

22. Speijer D. Oxygen radicals shaping evolution: why fatty acid catabolism leads to peroxisomes while neurons do without it: FADH(2)/NADH flux ratios determining mitochondrial radical formation were crucial for the eukaryotic invention of peroxisomes and catabolic tissue differentiation. *BioEssays : news and reviews in molecular, cellular and developmental biology* 2011, **33**(2)**:** 88-94.

23. Benard G, Faustin B, Galinier A, Rocher C, Bellance N, Smolkova K*, et al.* Functional dynamic compartmentalization of respiratory chain intermediate substrates: implications for the control of energy production and mitochondrial diseases. *The international journal of biochemistry & cell biology* 2008, **40**(8)**:** 1543-1554.

24. Mracek T, Drahota Z, Houstek J. The function and the role of the mitochondrial glycerol-3-phosphate dehydrogenase in mammalian tissues. *Biochimica et biophysica acta* 2013, **1827**(3)**:** 401-410.

25. West AP, Brodsky IE, Rahner C, Woo DK, Erdjument-Bromage H, Tempst P*, et al.* TLR signalling augments macrophage bactericidal activity through mitochondrial ROS. *Nature* 2011, **472**(7344)**:** 476-480.

26. Kelso GF, Porteous CM, Coulter CV, Hughes G, Porteous WK, Ledgerwood EC*, et al.* Selective targeting of a redox-active ubiquinone to mitochondria within cells: antioxidant and antiapoptotic properties. *The Journal of biological chemistry* 2001, **276**(7)**:** 4588-4596.

27. Nunes P, Demaurex N, Dinauer MC. Regulation of the NADPH oxidase and associated ion fluxes during phagocytosis. *Traffic* 2013, **14**(11)**:** 1118-1131.

28. Acin-Perez R, Carrascoso I, Baixauli F, Roche-Molina M, Latorre-Pellicer A, Fernandez-Silva P*, et al.* ROS-Triggered Phosphorylation of Complex II by Fgr Kinase Regulates Cellular Adaptation to Fuel Use. *Cell metabolism* 2014.

29. Nath AK, Ryu JH, Jin YN, Roberts LD, Dejam A, Gerszten RE*, et al.* PTPMT1 Inhibition Lowers Glucose through Succinate Dehydrogenase Phosphorylation. *Cell reports* 2015.

30. Lowell CA. Src-family kinases: rheostats of immune cell signaling. *Molecular immunology* 2004, **41**(6-7)**:** 631-643.

31. Alston TA, Mela L, Bright HJ. 3-Nitropropionate, the toxic substance of Indigofera, is a suicide inactivator of succinate dehydrogenase. *Proceedings of the National Academy of Sciences of the United States of America* 1977, **74**(9)**:** 3767-3771.

32. Gutman M. Modulation of mitochondrial succinate dehydrogenase activity, mechanism and function. *Mol Cell Biochem* 1978, **20**(1)**:** 41-60.

33. Pan H, Wu X. Hypoxia attenuates inflammatory mediators production induced by Acanthamoeba via Toll-like receptor 4 signaling in human corneal epithelial cells. *Biochemical and biophysical research communications* 2012, **420**(3)**:** 685-691.

34. Vance RE, Isberg RR, Portnoy DA. Patterns of pathogenesis: discrimination of pathogenic and nonpathogenic microbes by the innate immune system. *Cell host & microbe* 2009, **6**(1)**:** 10-21.

35. Sander LE, Davis MJ, Boekschoten MV, Amsen D, Dascher CC, Ryffel B*, et al.* Detection of prokaryotic mRNA signifies microbial viability and promotes immunity. *Nature* 2011, **474**(7351)**:** 385-389.

36. Kanneganti TD, Ozoren N, Body-Malapel M, Amer A, Park JH, Franchi L*, et al.* Bacterial RNA and small antiviral compounds activate caspase-1 through cryopyrin/Nalp3. *Nature* 2006, **440**(7081)**:** 233-236.

37. Sokolovska A, Becker CE, Ip WK, Rathinam VA, Brudner M, Paquette N*, et al.* Activation of caspase-1 by the NLRP3 inflammasome regulates the NADPH oxidase NOX2 to control phagosome function. *Nature immunology* 2013, **14**(6)**:** 543-553.

38. Acin-Perez R, Bayona-Bafaluy MP, Fernandez-Silva P, Moreno-Loshuertos R, Perez-Martos A, Bruno C*, et al.* Respiratory complex III is required to maintain complex I in mammalian mitochondria. *Mol Cell* 2004, **13**(6)**:** 805-815.

39. Diaz F, Fukui H, Garcia S, Moraes CT. Cytochrome c oxidase is required for the assembly/stability of respiratory complex I in mouse fibroblasts. *Mol Cell Biol* 2006, **26**(13)**:** 4872-4881.

40. Guaras A, Perales-Clemente E, Calvo E, Acin-Perez R, Loureiro-Lopez M, Pujol C*, et al.* The CoQH2/CoQ Ratio Serves as a Sensor of Respiratory Chain Efficiency. *Cell reports* 2016, **15**(1)**:** 197-209.

41. Huang YL, Morales-Rosado J, Ray J, Myers TG, Kho T, Lu M*, et al.* Toll-like receptor agonists promote prolonged triglyceride storage in macrophages. *The Journal of biological chemistry* 2014, **289**(5)**:** 3001-3012.

42. Geng J, Sun X, Wang P, Zhang S, Wang X, Wu H*, et al.* Kinases Mst1 and Mst2 positively regulate phagocytic induction of reactive oxygen species and bactericidal activity. *Nature immunology* 2015, **16**(11)**:** 1142-1152.

43. Kuida K, Lippke JA, Ku G, Harding MW, Livingston DJ, Su MS*, et al.* Altered cytokine export and apoptosis in mice deficient in interleukin-1 beta converting enzyme. *Science* 1995, **267**(5206)**:** 2000-2003.

44. Martinon F, Petrilli V, Mayor A, Tardivel A, Tschopp J. Gout-associated uric acid crystals activate the NALP3 inflammasome. *Nature* 2006, **440**(7081)**:** 237-241.

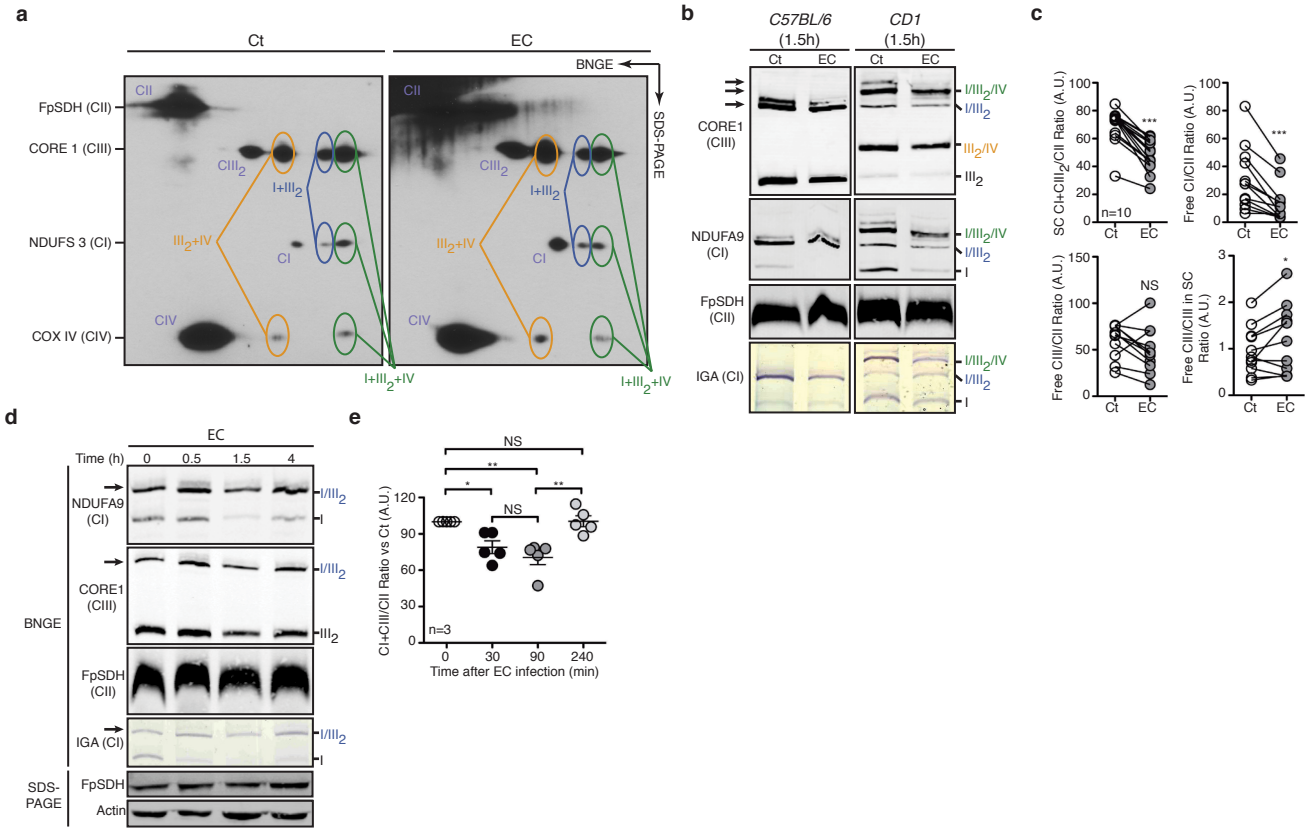

Figure 1 Detection of bacteria decreases the abundance of mitochondrial electron transport chain complex I (CI) and CI-containing supercomplexes. (**a**) Two-dimensional gel immunoblot analysis of mitochondria isolated from BMDMs stimulated with medium (Ct) or viable *E. coli* (EC) for 1.5h. One representative of 3 experiments is shown. Circles indicate localization of the different complexes. (**b, d**) Blue-native gel electrophoresis (BN-PAGE) immunoblot and in-gel activity (IGA) assay of CI in mitochondria isolated from *CD1* BMDMs (**b**) and *C57BL/6J* BMDMs (**b, d**) stimulated with EC for the indicated time. (**c**) Densitometric analysis of 'CI+$CIII_2$/CII', 'free CI/CII', 'free CIII/CII' and 'free CIII/CIII in SC' signal ratio as observed by BNGE immunoblot of *C57BL/6J* BMDMs treated as in (**b**). NS, not significant; *P < 0.05; ***P<0.001 by paired t-test analysis. (**e**) Densitometric analysis of BN-PAGE showing CI+CIII SC proportion *vs*. CII as observed by BNGE immunoblot of *C57BL/6J* BMDMs treated as in (**d**). NS, not significant; *P < 0.05; **P < 0.01 by one-way ANOVA followed by Tukey post-test analysis. Data present mean +/- s.e.m. of 3 independent experiments. Immunoblot membranes were probed with the indicated mETC-subunit-specific antibodies (**a, b, d**). Arrows indicate the main SCs affected (**b, d**).

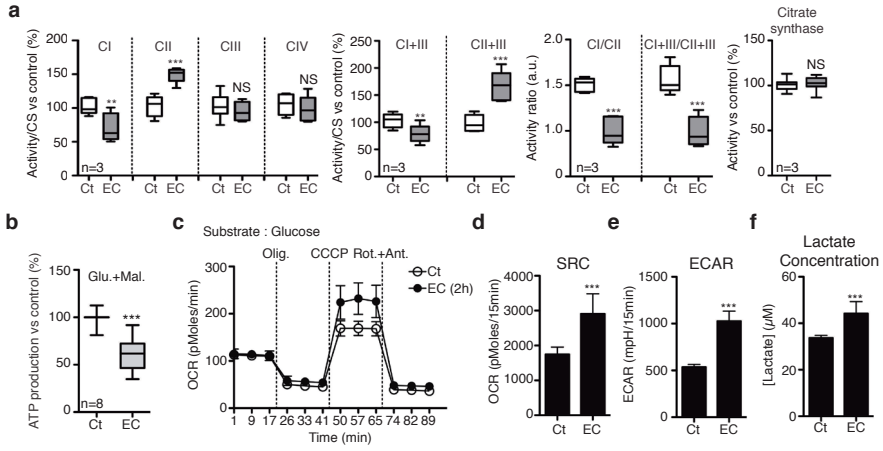

Figure 2 Detection of bacteria induces changes in mitochondrial ETC complex activities and influences mitochondrial respiration and glycolysis. (**a**) Spectrophotometric activities of the indicated mitochondrial respiratory complexes, normalized to citrate synthase (CS) activity in mitochondria isolated from BMDMs treated or not with *E. coli* for 1.5h. (**b**) Effect of EC-stimulation on *C57BL/6J* BMDM glutamate+malate-driven ATP synthesis. (**c-f**) Oxygen consumption rate (OCR) upon sequential treatment of oligomycin (olig.), CCCP, and rotenone+antimycin (Rot.+Ant.) (**c**), spare respiratory capacity (SRC) (**d**), basal extracellular acidification rate (ECAR) (**e**) and extracellular lactate concentration (**f**) in *C57BL/6J* BMDMs treated or not with EC for 2h. Error bars, s.e.m. NS, not significant; **P < 0.01; ***P < 0.001 by two-tailed unpaired t-test. Data (**a, b, d, e, f**) are means +/- s.e.m. of 3-to-8 independent experiments performed in 3 to 5 technical replicates. Data in **c** are means +/- s.e.m. of 4 to 5 technical replicates from one representative of 3 independent experiments.

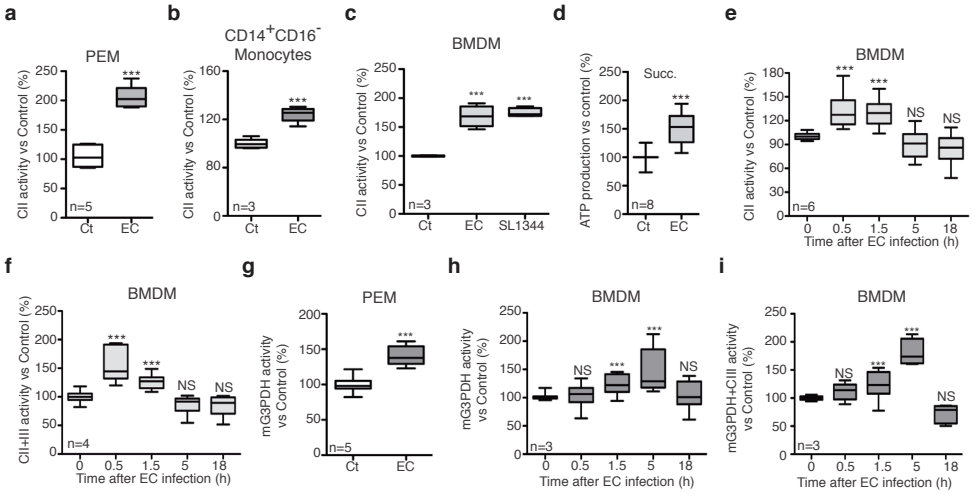

Figure 3 Sensing of bacteria transiently induces mitochondrial complex II and glycerol-3-phosphate dehydrogenase activities. (**a, b, c, e, f**) CII activity (**a, b, c, e**) and CII+CIII activity (**f**) in thioglycollate-elicited *C57BL/6J* macrophages (**d**), human CD14^{+}CD16^{-} monocytes (**e**), or *C57BL/6J* BMDM (**c, e, f**) stimulated with EC or *S. enterica* Typhimurium (SL1344) (**c**) for 1.5h or for the indicated time. (**d**) Succinate (Succ)-driven ATP synthesis in *C57BL/6J* BMDM stimulated with EC for 1.5h. (**g-i**) Mitochondrial glycerol-3-phosphate dehydrogenase (mG3PDH) (**g, h**) and G3PDH+CIII (**i**) in thioglycollate-elicited *C57BL/6J* macrophages (**g**) or *C57BL/6J* BMDM (**h, i**) stimulated with EC for 1.5h or for the indicated time. Error bars, s.e.m. NS, not significant; ***P < 0.001 by two-tailed unpaired t-test. Data are means +/- s.e.m. of 3 to 8 independent experiments performed in 3 to 5 technical replicates.

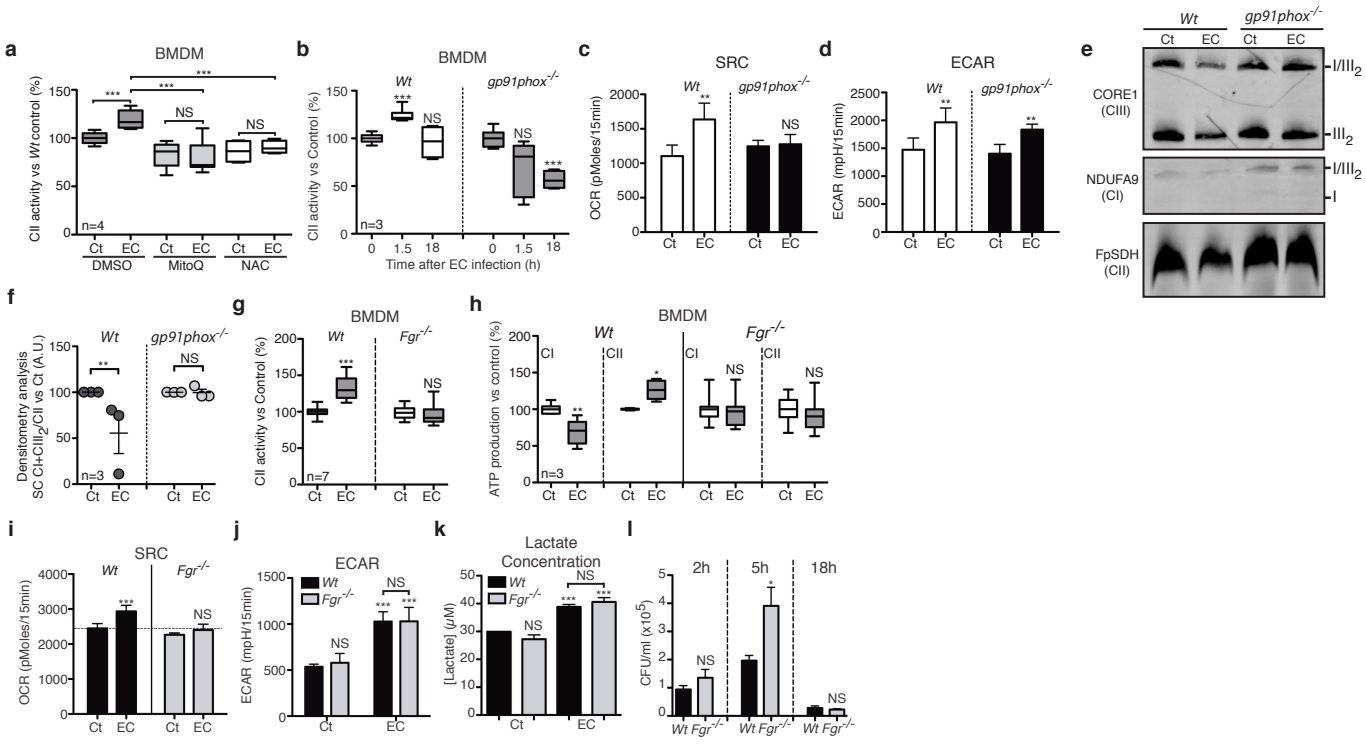

Figure 4 Induction of mitochondrial complex II activity upon detection of *E. coli* relies on phagosomal reactive oxygen species (ROS) and the ROS-dependent Fgr kinase. (**a, b**) CII activity in *C57BL/6J* and *gp91phox*$^{-/-}$ BMDMs stimulated with EC for 1.5h and treated with the ROS inhibitors N-acetylcysteine (NAC) or mitoQ (**a**). (**c, d**) spare respiratory capacity (SRC) (**c**) and extracellular acidification rate (ECAR) (**d**) in *gp91phox*$^{-/-}$ and *Wt* BMDMs stimulated with EC for 2h. (**e**) BNGE immunoblot of mitochondria isolated from *gp91phox*$^{-/-}$ and *Wt* BMDMs stimulated with EC for 2h. Representative of 3 independent experiments. (**f**) Densitometric analysis of BN-PAGE showing CI+CIII SC proportion *vs*. CII. (**g-k**) Effect of *E. coli*-stimulation on CII activity (**g**), substrate-driven ATP synthesis (**h**), SRC (**i**), and ECAR (**i**) and extracellular lactate concentration (**k**) of *Fgr*$^{-/-}$ and *Wt* BMDMs. (**l**) Intracellular colony-forming units (CFU) after EC-infection of *Fgr*$^{-/-}$ and *Wt* BMDMs for the indicated times at MOI = 5. Error bars, s.e.m. NS, not significant; *P < 0.05; **P < 0.01; ***P < 0.001 by two-tailed unpaired t-test. Data are means +/- s.e.m. of 2 to 7 independent experiments performed in 3 to 5 technical replicates (**a-d, f-l**).

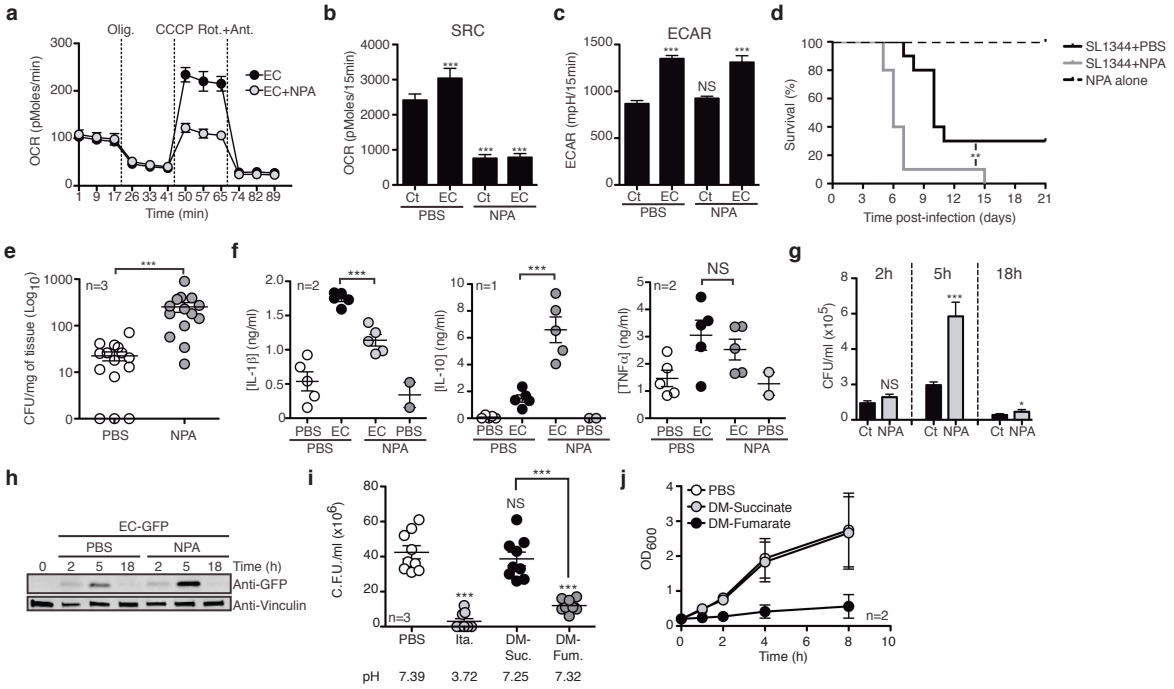

Figure 5 Mitochondrial complex II activity contributes to macrophage bactericidal capacity. (**a-c**) OCR upon sequential treatment with oligomycin (olig.), CCCP, and rotenone+antimycin (Rot.+Ant.) (**a**), SRC (**b**), and ECAR (**c**) in *C57BL/6J* BMDMs stimulated for 2h with EC +/- 3-nitropropionic (NPA). (**d**) Survival of *C57BL/6J* mice infected with $1x10^9$ *S. enterica* Typhimurium by gavage and treated or not with 50mg/kg NPA every second day (n=10 per group). **P < 0.01 by Log-rank (Mantel-Cox) test. (**e, f**) Splenic bacterial burdens 72h after intra-peritoneal injection of 1 x 10^8 of viable *E. coli* (**e**), and serum levels of IL-1β, IL-10 and TNFα 2h after intra-peritoneal injection of 1 x 10^9 of viable *E. coli* (**f**) into *C57BL/6J* mice treated or not with 50mg/kg NPA are shown. Each symbol represents one mouse. (**g, h**) Intracellular CFUs (**g**) and anti-GFP immunoblot of SDS-solubilized extracts (**h**) from *C57BL/6J* BMDMs treated or not with NPA and infected with *E. coli* (**g**) or GFP-expressing *E. coli* (**h**) at MOI = 5 for the indicated times. (**i**) CFUs of *E. coli* incubated 3h with 10mM itaconic acid, dimethyl (DM)-succinate or DM-fumarate and grown overnight on a Petri dish. (**j**) *S. enterica* Typhimurium growth in lysogeny broth (LB) supplemented with 10mM of the indicated reagent. Error bars, s.e.m. NS, not significant; *P < 0.05; **P < 0.01; ***P < 0.001 by two-tailed unpaired t-test. Data are means +/- s.e.m. of 2 to 3 independent experiments performed in 2 to 5 technical replicates (**b-g, i, j**). Data in **a** are means +/- s.e.m. of 4 to 5 technical replicates from one representative of at least 3 independent experiments.

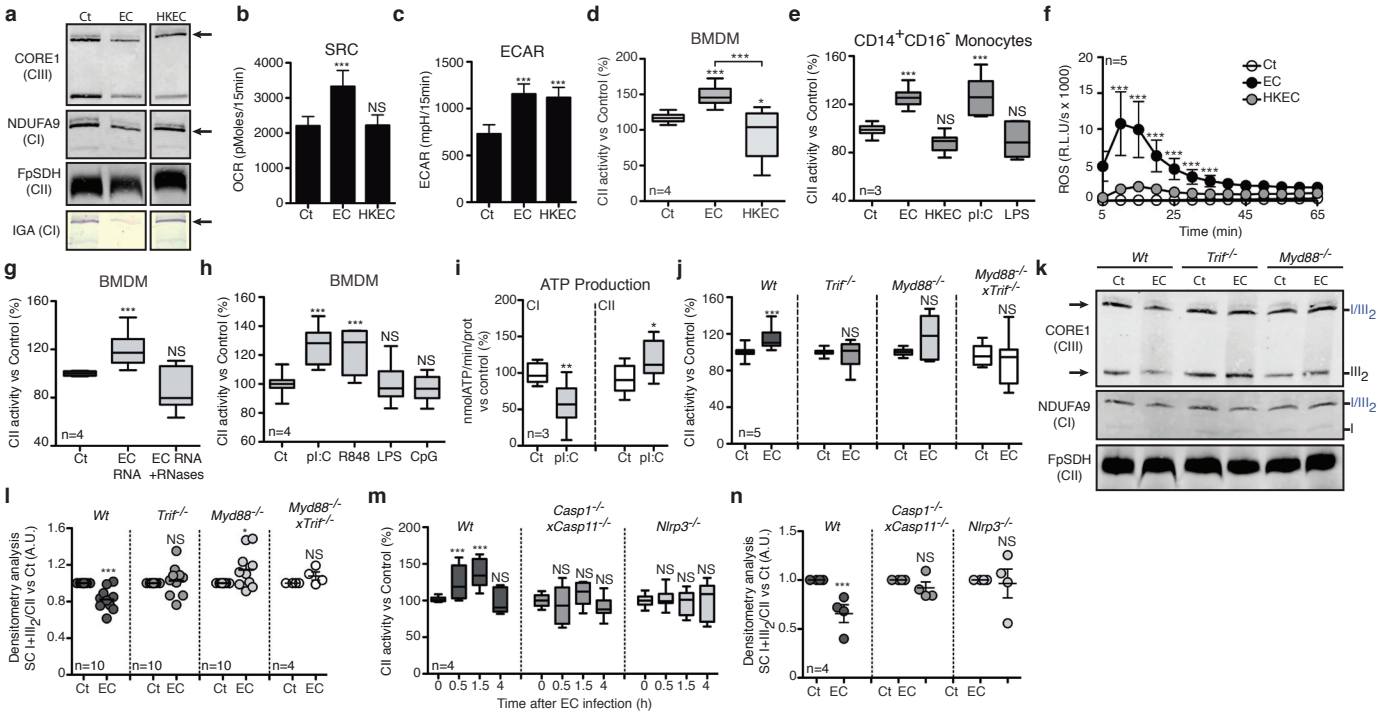

Figure 6 Sensing of bacterial viability induces TLR- and NLRP3 inflammasome-dependent decrease in CI and CI-containing supercomplexe abundance and increase in CII activity. (**a**) BN-PAGE immunoblot analysis and CI-in gel activity (IGA) assay in BMDMs treated as indicated. (**b-e**) SRC (**b**), ECAR (**c**) and CII activity (**d, e**) in BMDMs (**b-d**) and human $CD14^+$ monocytes (**e**) stimulated with EC or HKEC are shown. (**f**) ROS production by BMDMs stimulated as in (**b**). (**g, h**) CII activity in *Wt* BMDMs stimulated as indicated for 1.5h. (**i**) Substrate-driven ATP synthesis assay in BMDMs stimulated with pI:C. (**j**) CII activity in *Wt*, *Trif*$^{-/-}$, *Myd88*$^{-/-}$ and *Trif*$^{-/-}$x*Myd88*$^{-/-}$ BMDMs treated as indicated. (**k**) BN-PAGE immunoblot analysis of resting and *E. coli*-stimulated *Wt*, *Trif*$^{-/-}$ and *Myd88*$^{-/-}$ BMDMs. Arrow indicate the main SCs affected. (**l, n**) Densitometric analysis of CI+$CIII_2$/CII signal ratio as observed by BNGE immunoblot of BMDMs of the indicated genotype stimulated with EC for 1.5h. (**m**) CII activity in *Wt*, *Nlrp3*$^{-/-}$ and *Caspase1*$^{-/-}$x*Caspase11*$^{-/-}$ BMDMs stimulated with EC for the indicated time point. Poly(I:C), (pI:C); LPS, lipopolysaccharide; CpG, CpG oligodeoxynucleotide. Error bars, s.e.m. NS, not statistically significant; *P < 0.05; **P < 0.01; ***P < 0.001 by two-tailed unpaired t-test. Data are means +/- s.e.m. of 3 to 4 independent experiments performed in 2-5 replicates (**b-j, l-n**).

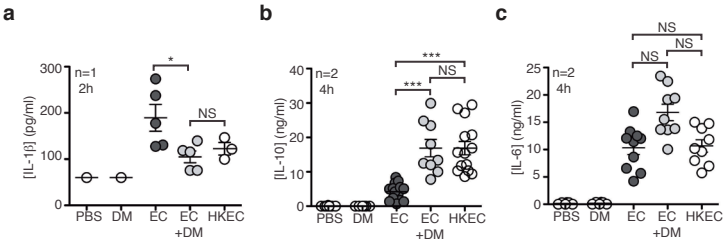

Figure 7 Inhibition of CII *in vivo* modulates cytokines production upon viable *E. coli* challenge. (**a-c**) Serum levels of IL-6 (**a**), IL-10 (**b**) and IL-1β (**c**) at the indicated time point after intra-peritoneal injection of $1x10^9$ viable EC or $1x10^{10}$ HKEC in Wt mice treated or not with dimethyl-Malonate (DM). Poly(I:C), (pI:C); LPS, lipopolysaccharide; CpG, CpG oligodeoxynucleotide. Error bars, s.e.m. NS, not statistically significant; *P < 0.05; **P < 0.01; ***P < 0.001 by two-tailed unpaired t-test. Each symbol represent one mouse. Data are means +/- s.e.m. of 1 representative experiment (**b, a**). Data are means +/- s.e.m. of 2 independent experiments (**b, c**).

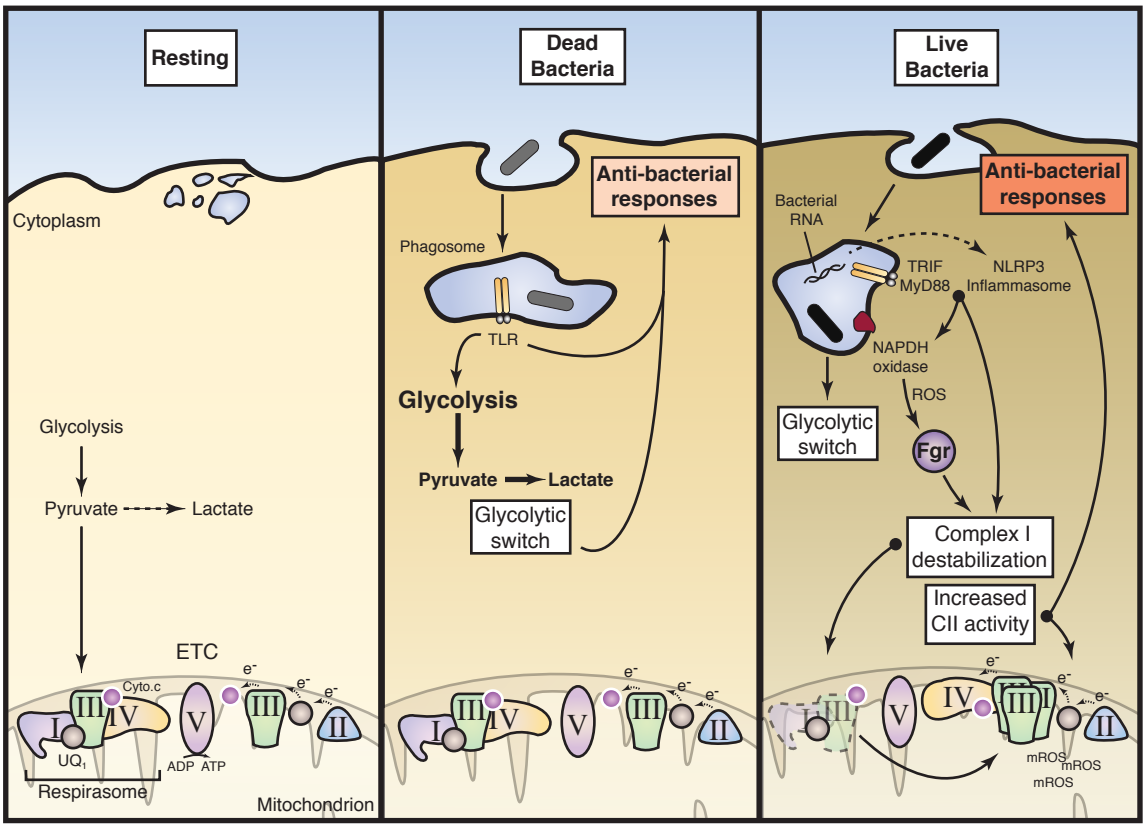

Figure 8 Schematic representation of the consequences of bacteria detection on macrophage mitochondrial respiratory chain and metabolism. In resting macrophages, glycolytic flux generates pyruvate that feeds the TCA cycle for oxidative phosphorylation through the respirasome (CI+$CIII_2$+CIV). TLR signaling generated by the detection of bacteria increases glycolytic flux but pyruvate is diverted from entering the mitochondria for oxidative phosphorylation. Presence of bacterial RNA betray bacteria viability and innate immune signaling takes place involving the Toll-like receptor adaptors TIR-domain-containing adapter-inducing interferon-β (TRIF) and myeloid differentiation primary response 88 (MyD88), the NOD-like receptor (NLR) family, pyrin domain-containing protein 3 (NLRP3) inflammasome, and the phagosomal NADPH oxidase. Reactive oxygen species (ROS)-dependent Fgr kinase then transiently affect the ETC characterized by provoking a disassembly of CI and the respirasome and increases CII activity that compensates for CI-activity decrease. This may release CIII from its association to CI to make it available for electrons provided by CII, the activity of which potentiates anti-microbial responses against viable bacteria. ETC, electron transport chain ; UQ_1, ubiquinone (co-enzyme Q) ; Cyto. c, cytochrome c ; e^-, electrons. ROS, reactive oxygen species.

ON LINE METHODS

Mouse strains. C57BL/6J and CD1 mice were purchased from Harlan Laboratories. *Myd88*$^{-/-}$ and *Trif*$^{/-}$ mice were originally generated by S. Akira and bred to homozygosity to generate *Trif*$^{/-}$*Myd88*$^{-/-}$ mice by R. Medzhitov. *Myd88*$^{-/-}$, *Trif*$^{/-}$ and *Trif*$^{/-}$*Myd88*$^{-/-}$ bone marrow cells were provided by J. Magarian Blander. *Ips1*$^{-/-}$ mice were originally obtained from S. Akira and backcrossed with *Trif*$^{/-}$ mice to obtain *Ips1*$^{-/-}$x*Trif*$^{/-}$ mice. C57BL/6J-Tmem173gt/J mice (hereafter GT-Sting mice) and *gp91phox*$^{-/-}$ (B6.129S6-Cybb^{tm1Din}/J) mice were obtained from the Jackson Laboratory. *Nlrp3*$^{-/-}$ and *Casp1*$^{-/-}$*Casp11*$^{-/-}$ mice have been described previously[43, 44]. We used 8- to 10-week-old animals (males or females) for all experiments. Experiments were repeated 3 times and 3-5 animals per group were used to reach statistical significance. No blinding or randomization strategy was used and no animal was excluded from analysis. All experimental procedures were approved by institutional care and use committees and performed in agreement with EU directive 86/609/EEC and recommendation 2007/526/EC regarding the protection of laboratory animals and enforced under Spanish law by Royal decree 1201/2005.

Reagents. Lipopolysaccharide, polyinosinic:polycytidylic acid (polyI:C), CpG ODN were purchased from Invivogen. 3-nitropropionic acid (NPA), succinate, succinate hexahydrate, glutamate, malate disodium-salt, fumarate, dimethyl-fumarate, dimethyl succinate, dimethyl malonate (DM), itaconic acid, thenoyltrifluoroacetone (TTFA), carbonilcyanide p-triflouromethoxyphenylhydrazone (FCCP), CCCP, oligomycin, rotenone, antimycin A, ubiquinone, sn-glycerol 3-phosphate, oxidized cytochrome c, adenosine tri-phosphate (ATP), adenosine di-phosphate (ADP), phenazine methosulfate (PMS) and digitonin were all from Sigma. Antibodies for FACS were all from BD Biosciences except for F4/80 phycoerythrin (PE)-antibody, which was from eBioscience. Luciferin and luciferase were from Promega and Roche, respectively.

Bacteria. *Escherichia coli* K12, strain DH5α, were purchased from Invitrogen. *Salmonella enterica* serovar Thyphimurium strain SL1344 were provided by F. Norel-Bozouklian. SL1344 were grown in LB broth supplemented with 50μg/ml streptomycin (Sigma). For phagocytosis experiments, bacteria were grown overnight in Luria-Bertani (LB) broth with shaking, diluted 1/50, and grown until log-phase [optical density at 600 nm (OD_{600}) of 0.8-1.2] without shaking. Bacteria were washed with phosphate buffer

saline (PBS) to remove LB salts before addition to cells. For heat-killing, *E. coli* (HKEC) were grown to log phase, washed, re-suspended in PBS and subsequently incubated at 60˚C for 60-90 min. Aliquots of heat-killed bacteria were stored at -80˚C until use. Efficient killing was confirmed by overnight plating on LB-agar plates. Total RNA was isolated from E. coli using the e.z.n.a. Bacterial RNA kit (Omega Bio-Tek). *E. coli*-GFP were generated by transformation of BL21pLysS bacteria (Invitrogen) with a pET-28 vector encoding the GFP-OT fusion protein[45]. *E. coli*-GFP were grown in the presence of 50 μg/ml kanamycin and 50 μg/ml chloramphenicol. To induce GFP expression, overnight-grown bacteria were diluted to an OD_{600} of 0.8 and incubated for 4h in the presence of 1 mM Isopropyl β-D-1-thiogalactopyranoside (IPTG).

Antimicrobial assay. The following bacteria strains were used: *Salmonella enterica* serovar Thyphimurium strain SL1344, *Escherichia coli* K12, strain DH5α (Invitrogen). Bacteria were cultured at 37 °C overnight in lysogeny broth (LB). Bacterial concentrations were measured by spectrophotometry at 600 nm and diluted to a concentration of 10^5 CFU/ml in PBS supplemented with 0.1, 1, or 10mM of itaconate, fumarate, succinate, dimethyl-fumarate or dimethyl-succinate and incubate for 6h at room temperature. Serial dilutions were then plated on LB-agar plates supplemented with 50mM streptomycin (for SL1344) and grown overnight at 37˚C. Photographs were taken using a scanner. Alternatively, bacteria were diluted to a final OD600=0.2 in LB supplemented as above and growth was measured every 2h by spectrophotometry. For CFU enumeration, bacteria were diluted to a concentration of 10^5 CFU/ml in PBS supplemented as above, incubated for 6h and serial dilution were plated on LB-agar plates. The number of colonies formed after overnight incubation was counted. For analysis of cell death, bacteria were stained with 5μM propidium iodide (to stain nucleic acids) and 5μM of cell SYTO red dye (Life Technology) for 15min, and analyzed by flow cytometry.

Macrophage preparation and treatment with *Escherichia coli*. Murine bone marrow-derived macrophages (BMDMs) were generated from *C57BL/6J, CD1, Fgr*$^{-/-}$*, Myd88*$^{-/-}$*, Trif*$^{-/-}$*, Trif*$^{-/-}$*/Myd88*$^{-/-}$*, GT-sting, Ips-1, Trif*$^{-/-}$x*Ips-1*$^{-/-}$, *gp91phox*$^{-/-}$*, Nlrp3*$^{-/-}$ and *Casp1*$^{-/-}$

Casp11$^{-/-}$ mice, as described previously[46], in RPMI 1640 supplemented with M-CSF (30% mycoplasma-free L929 cell supernatant, NCBI Biosample accession # SAMN00155972) and 10% FBS, plus 100 µg/ml penicillin, 100 µg/ml streptomycin, 10 mM HEPES, 1 nM sodium pyruvate and 50 mM 2-mercaptoethanol (all from Gibco). Peritoneal macrophages were harvested 72h after intraperitoneal injection of 1 ml 3% thioglycollate medium (BD Bioscience). Human $CD14^{+}CD16^{-}$ monocytes were obtained from buffy coats using the EasySep Human Monocyte Enrichment Immunomagnetic kit (Stemcell Technologies). For treatment with viable *E. coli* and HKEC, cells were plated at $1.5x10^{6}$ cells/well in non-treated 6-well cell culture plates (BD Bioscience) and left to adhere for at least 4h. BMDMs were challenged with *E. coli* or HKEC at a multiplicity of infection (MOI) of 20 and plates were spun at 400 *g* for 5min. Cells were incubated for 1.5h unless otherwise indicated. For longer time points, 50 µg/ml gentamicin sulfate (Gibco) was added after 1h incubation. Alternatively, cells were stimulated with soluble ligands as follows: 200 ng/ml LPS, 20 µg/ml poly(I:C), 5 µg/ml CpG ODN. For treatment with metabolic inhibitors, 0.5 mM 3-nitropropionic acid (NPA), 0.5mM dimethyl-fumarate or 0.5mM TTFA were added to the cells 30 min-to-1 h prior challenge. For stimulation of human, $CD14^{+}$ $CD16^{-}$ monocytes were isolated from buffy coats. Cells were plated at $1x10^{6}$ cells/ml in non-treated 12-well cell culture plates (BD Bioscience) and left to adhere for at least 2h. Cells were challenged with E. coli and HKEC at a multiplicity of infection (MOI) of 10 and plates were spin at 2500rpm for 1min. Cells were incubated for 1.5h. Alternatively, cells were stimulated with soluble ligands as follows: 250 ng/ml Ultrapure EK-LPS and 10 µg/ml LMW poly(I:C). For supernatant collection, cells were plated at $3x10^{5}$ cells/well in a 48-well plate and stimulated as described above.

Oxygen consumption rate and glycolytic flux evaluation. Real-time oxygen consumption rate (OCR) and extracellular acidification rate (ECAR) in BMDMs were determined with an XF-96 Extracellular Flux Analyzer (Seahorse Bioscience); $1x10^{5}$ cells/well in 5-6 wells were used for each condition. The assay was performed in DMEM supplemented with 2mM glutamine, 100 µg/ml penicillin, 100 µg/ml streptomycin, phenol red and 25 mM glucose + 1mM pyruvate or 5 mM L-carnitine + 50 µM palmitoyl-CoA. The pH was adjusted to 7.4 with KOH (herein called seahorse medium).

Three consecutive measurements were performed under basal conditions and after the sequential addition of the following ETC inhibitors: 1µM oligomycin, 1 µM CCCP, 1 µM rotenone and 1 µM antimycin. Basal respiration rate (BRR) was defined as OCR in the absence of any inhibitor. Maximal respiration rate (MRR) was defined as the OCR after addition of oligomycin and FCCP. Spare respiration capacity (SRC) was defined as the difference between MRR and BRR. ECAR was measured in the absence of drug. Where indicated, cells were treated with 0.5 mM NPA for 30 min prior to stimulation. For lactate production measurement, cells ($1x10^5$/well) were plated on a 96-well plate and stimulated as indicated. Cells were washed 5 times with PBS and 100µl of seahorse medium was added. Plates were incubated at 37˚C without CO_2 for 1h and supernatants were harvested. 25µl of 5-time-diluted supernatant was use to measure lactate production using a Lactate assay kit II (Sigma) according to manufacturer's instructions.

Isolation of mitochondria and BMDM permeabilization. Mitochondria were isolated as described by Schägger *et al.*[47] with some modifications. $1x10^8$ BMDMs were collected in PBS supplemented with 5 mM EDTA and washed with PBS. Cell pellets were frozen at -80˚C to increase cell breakage and were homogenized in a tightly fitting glass-teflon homogenizer with 10 volumes of buffer A (83mM sucrose, 10 mM MOPS, pH 7.2). An equal volume of buffer B (250 mM sucrose, 30 mM MOPS, pH 7.2) was added and nuclei and unbroken cells were removed by centrifugation at 1000 *g* for 5 minutes. Supernatants were collected and centrifuged at 12 000 g for 2 min. Mitochondria pellets were washed once with buffer C (320 mM sucrose, EDTA 1 mM, 10 mM Tris-HCl, pH 7.4). Mitochondria were then suspended in an appropriate volume of PBS for storage at -80˚C.

Blue-native polyacrylamide gel electrophoresis (BN-PAGE), two-dimensional gel analysis, and in gel activity assay. For BMDMs permeabilization, $3x10^6$ macrophages were resuspended in 100 µl of PBS. 32.5 µl of digitonin (8 mg/ml) was added and cells incubated on ice for 10 min. Cold PBS (1 ml) was added and cells were centrifuged for 5 min at 10 000 *g*. The pellet was suspended in 100 µl of AA buffer (500 mM 6-aminohexanoic acid, 50 mM immidazole, 1 mM EDTA, pH 7) and 10 µl of a 10% digitonin solution was added. Cells were centrifuged for 30 min at 18 000 *g*. Supernatant was harvested and 10 µl of sample buffer (5% Blue G-250, 5% glycerol in AA Buffer)

was added. Samples were stored at -80˚C until use. BN-PAGE was performed as described by Wittig *et al.*[48]. For 2-dimensional gel analysis, 50 to 75 µg of mitochondria were digitonin-permeabilized with 4 µg digitonin per µg of protein and loaded on a BN polyacrylamide gel. Each individual band on the BN-PAGE was cut out and incubated for 1 hour in buffer containing 1% SDS and 1% 2-mercaptoethanol. The buffer was replaced with a 1% SDS solution and incubation was continued for 30 min. BN-PAGE bands were loaded on an SDS polyacrylamide gel composed of a 10% acrylamide/Bis-acrylamide (AB) stacking gel and a 16% AB resolving gel. Electrophoresis was performed overnight at 12-to-15 mA, and proteins were transferred to a PVDF membrane using a Trans-Blot Semi-Dry Transfer Cell (Bio-Rad). For in-gel OXPHOS complex activity assays, CI was revealed by incubating the BN gel for 1h-to-3h in 0.1M Tris-HCl, pH 7.5, containing 1mg/ml NBT and 0.14mM NADH. For densitometry analysis, the ImageJ64 software was used. Band limits were determined using low exposure images to efficiently distinguish the different bands. Background correction was applied for each analysis.

OXPHOS function and enzyme activities. CII activity was measured spectrophotometrically from the reduction of 2,6-diclorophenol-indophenol (DCPIP) by tracking the absorbance at 600 nm over 3min as described[49] with some modifications. Briefly, $3x10^6$ cells were suspended in 100µl PBS on ice. Protein concentration was determined and the volume was adjusted to the lowest concentrated sample. Sample (20 µl) was suspended in 950 µl of buffer C1/C2 (25 mM potassium phosphate (K_2HPO_4) pH=7.2, 5 mM $MgCl_2$, 3 mM KCN, 2.5 mg/ml BSA) supplemented with 100 mM succinate and 0.1% Triton X-100, and incubated 10 min at room temperature in a cuvette. After addition of 6 µl 5 mM DCPIP, 2 µl 1 mg/ml of antimycin A and 2 µl 1 mM rotenone, samples were incubated for 2 min. Then, 6 µl of 10 mM UQ_1 was added and absorbance was measured. CII activity was extrapolated using the following formula: [CII Activity = ((rate/min)/19.1) / sample volume x 1000 x dilution factor], where 19.1 is the molar extinction coefficient at 30˚C ($mM^{-1}cm^{-1}$). For CII+CIII, UQ_1 was replaced with 1 mM oxidized cytochrome c (Sigma). For SDH activity, UQ_1 was replaced with phenazine methosulfate (PMS). For mitochondrial glycerol 3-phosphate dehydrogenase (mG3PDH) activity, succinate was replaced with 1 M glycerol-3-phosphate. For

OXPHOS enzymatic activities in isolated mitochondria, individual and combined complex activities of isolated mitochondria were measured spectrophotometrically as described[49].

ATP synthesis assay. ATP synthesis was measured in permeabilized cells by kinetic luminescence assay[50]. Cells ($2x10^6$) were suspended in 160 µl of buffer A (150mM KCl, 25mM Tris-HCl, 2mM EDTA, 0.1% BSA FA, 10mM K-phosphate, 0.1mM MgCl2, pH 7.4) at room temperature (RT) and 50 µg/ml digitonin was added. Samples were mixed gently for 1 min, and the reaction was stopped by addition of 1ml of buffer A. Cells were centrifuged at 3000 rpm for 2 min at RT, and pellets were suspended in 160 µl of buffer A and dispensed into the wells of a 96-well luminescence reading plate (Costar). Substrate cocktail (50 µl) and 20 µl of buffer B (0.5M Tris-acetate, pH 7.75, 0.8mM luciferine, 20 µg/ml luciferase) were added, and luminescence was measured over 1 min. Substrate cocktails were composed of 6 mM diadenosin pentaphosphate and 6 mM ADP supplemented with 1 M glutamate + 1 M malate for determination of CI activity or with 1 M succinate for CII activity. All measurements were performed in triplicate.

Phagocytosis assay. Macrophages ($3x10^5$) were seeded in triplicate on a non-treated 24-well plate (BD Biosciences). Cells were challenged with $6x10^6$ 3µm Fluoresbrite®-microspheres (Polysciences) or $3x10^6$ *E. coli*-GFP and centrifuged for 5 min at 400 *g*. After 20 min incubation, cells were washed with PBS, harvested in PBS containing 5 mM EDTA, and analyzed by flow cytometry.

Cytokine enzyme-linked immunosorbent assay (ELISA). IL-1β, IL-10 and TNF-α ELISA kits were from BD Biosciences. Capture/detection antibodies for IL-6 antibodies were from BD Biosciences. Supernatants from BMDMs were collected at 24h after stimulation. ELISA kits are used according to the manufacturer's instructions. Detection antibodies were biotinylated and labeled with streptavidin-conjugated horseradish peroxidase (HRP, from invitrogen) and visualized by incubation with 5,5'-tetramethylbenzidine solution (TMB, KPL). Colour development was stopped with TMB-stop solution (KPL). Recombinant cytokines served as standards and were purchased from Peprotech. Absorbances at 450 nm were measured on a microplate reader (Benchmark Plus, Bio-Rad)

***In vitro* and *in vivo* infections and bactericidal activity experiments.** For *in vitro* experiments, BMDMs were plated at $2x10^5$ cells/well in triplicate on a 24-well plate in an antibiotic-free complete medium. BMDMs were infected with DH5α or SL1344 at a multiplicity of infection of 5 and centrifuged for 5 min at 400 *g*. After 30 min incubation, cells were washed and complete medium supplemented with 50 μg/ml gentamycin was added. At the indicated time point after infection, cells were washed with PBS and 1 ml of PBS containing 1% Triton X-100 was added. Plates were incubated at room temperature for 15 min and serial dilutions (1/10, 1/100, 1/1000) were plated on an LB-agar plate, which in the case of SL1344 contained 50 μg/ml streptomycin. Plates were incubated at 37˚C and bacterial colonies were counted. When needed, cells were pretreated with 3-nitropropionic acid (NPA) 30 min before infection; the inhibitor concentration was maintained throughout the experiment. For *in vivo* experiments, mice were injected intraperitoneally (i.p.) with 50mg/kg NPA 1 hour before infection. Injection of inhibitor was repeated every second day over the course of the experiment. For *E. coli* infection, mice were injected i.p. with $1x10^8$ DH5α and sacrificed at 72h post-infection. Spleens were harvested and homogenized in 5 ml PBS, and serial dilutions were plated on LB-agar plates for colony counting. For peritoneal cell analysis, mice were injected i.p. with $1x10^8$ DH5α. Twelve hours later, mice were sacrificed and peritoneal cells were collected in 8 ml ice-cold PBS. Each experiment included 4-5 mice per group and was repeated 3 times with similar results. No specific blinding or randomization strategy was used. No animal was excluded from analysis.

Immunoblot. For protein extract collection, $1.5x10^6$ cells were lysed in RIPA buffer supplemented with protease and phosphatase inhibitor cocktails (both from Roche) and subsequently sonicated and boiled for 5 min at 95˚C. Protein lysates were separated on 4-12% SDS-gradient gels (Bio-Rad). Proteins were transferred to PVDF membranes (Millipore). Membranes were blocked with 5% bovine serum albumin (BSA) in PBS and probed with antibodies sourced as follows: anti-CORE1, -NDUSF3, -ATP-B, and -NDUFA9 were from Abcam; anti-FpSDH was from Invitrogen; anti-Cox5b was from Proteintech Europe; anti-vinculin was from Sigma; and anti-β-actin was from Santa Cruz Biotechnology.

Real-time PCR. Total RNA was isolated from macrophages using the RNeasy kit

(Qiagen). Contaminating genomic DNA was removed by DNase digestion (Qiagen). Reverse transcription was performed using the High Capacity cDNA Reverse Transcriptase kit (Applied Biosystem), and cDNA was used for subsequent real-time PCR reactions. Quantitative real-time PCR was conducted on an 7900 HT Fast Real-Time PCR system (Lifetechnologies) using SYBR green qPCR Master Mix (Promega) with the following primer pairs: *β-Actin*, FW 5'- GAAGTCCCTCACCCTCCCAA-3', RV 5'-GGCATGGACGCGACCA-3'; *Il1b*, FW 5'-AAAGACGGCACACCCACCCTGC-3', RV 5'-TGTCCTGACCACTGTTGTTTCC CAG-3'; *Ifnb*, FW 5'- TCAGAATGAGTGGTGGTTGC ; RV 3'- GACCTTTCAAAT GCAGTAGATTCA; *Tnf* FW 5'-CCCCAAAGGGATGAGAAGTT, RV 3'-TGGGC TACAGGCTTGTCACT.

Flow cytometry. Cells were stained with the appropriate antibody cocktails in ice-cold PBS supplemented with 2 mM EDTA, 1% fetal calf serum and 0.2% sodium azide for 15min. Samples were processed by FACS canto-3L or LSR-Fortessa analyzers (BD Biosciences) and data were analyzed with FlowJo software.

Gene microarray analysis. Affymetrix Microarray data from BMDMs were previously deposited with the NCBI Gene Expression Omnibus under accession number GSE27960 by Sander *et al.*[35]. Data for genes encoding ETC subunits were analyzed and plotted using Genesis software from Graz university of Technology (http://genome.turgraz.at).

Statistical analysis. Statistical differences were analysed with Prism software (GraphPad Software Inc.). Statistical significance was tested by a two-tailed unpaired t-test. For survival experiments, statistical significance was tested by a Log-Rank (Mantel-Cox) test. Significance of differences is represented in the figures as follows: *, $P < 0.05$; **, $P < 0.01$; ***, $P < 0.001$. NS, not significant. Data are means +/- s.e.m. of 3-to-8 independent experiments performed in duplicates. Where indicated, data are means +/- s.e.m. of 4-to-5 technical replicates from one representative of at least 3 independent experiments.

45. Drutman SB, Trombetta ES. Dendritic cells continue to capture and present antigens after maturation in vivo. *J Immunol* 2010, **185**(4)**:** 2140-2146.

46. Blander JM, Medzhitov R. Regulation of phagosome maturation by signals from toll-like receptors. *Science* 2004, **304**(5673)**:** 1014-1018.

47. Schagger H, von Jagow G. Blue native electrophoresis for isolation of membrane protein complexes in enzymatically active form. *Analytical biochemistry* 1991, **199**(2)**:** 223-231.

48. Wittig I, Braun HP, Schagger H. Blue native PAGE. *Nature protocols* 2006, **1**(1)**:** 418-428.

49. Birch-Machin MA, Turnbull DM. Assaying mitochondrial respiratory complex activity in mitochondria isolated from human cells and tissues. *Methods in cell biology* 2001, **65:** 97-117.

50. Vives-Bauza C, Yang L, Manfredi G. Assay of mitochondrial ATP synthesis in animal cells and tissues. *Methods in cell biology* 2007, **80:** 155-171.

Supplementary Information

Host defence to bacteria involves adaptations of the mitochondrial respiratory chain in macrophages

Johan Garaude[1,2,8,9], Rebeca Acín-Pérez[1,8], Sarai Martínez-Cano[1], Michel Enamorado[1], Matteo Ugolini[3], Estanislao Nistal-Villán[4], Sandra Hervás-Stubbs[4,5], Pablo Pelegrín[6], Leif E. Sander[3], José A. Enríquez[1,7,9], & David Sancho[1,9]

[1]Centro Nacional de Investigaciones Cardiovasculares Carlos III (CNIC), Melchor Fernández Almagro, 3, 28029 Madrid, Spain.
[2]Institute for Regenerative Medicine and Biotherapies, Institut National pour la Santé et la Recherche Médicale, U1183, 80 Avenue Augustin Fliche, 34295 Montpellier Cedex 5, France.
[3]Department of Infectious Diseases and Pulmonary Medicine, Charité Hospital Berlin, Augustenburger Platz 1, 13352 Berlin, Germany.
[4]Centro de Investigación Médica Aplicada, Universidad de Navarra, Pio XII, 55 E-31008 Pamplona, Spain.
[5]Instituto de Investigación Sanitaria de Navarra (IDISNA), Recinto de Complejo Hospitalario de Navarra, E-31008, Pamplona, Spain.
[6]Unidad de Inflamación y Cirugía Experimental, Centro de Investigación Biomédica en Red en el Área Temática de Enfermedades Hepáticas y Digestivas, Hospital Clínico Universitario Virgen de la Arrixaca, Instituto Murciano de Investigación Biosanitaria-Arrixaca (IMIB-Arrixaca), 30120 Murcia, Spain.
[7]Departamento de Bioquímica y Biología Molecular y Celular. Universidad de Zaragoza. Zaragoza, Spain.
[8]These authors contributed equally to this work
[9]These authors jointly supervised this work
Correspondence and requests for materials should be addressed to J.G. (johan.garaude@inserm.fr), J.A.E (jaenriquez@cnic.es), or D.S (dsancho@cnic.es).

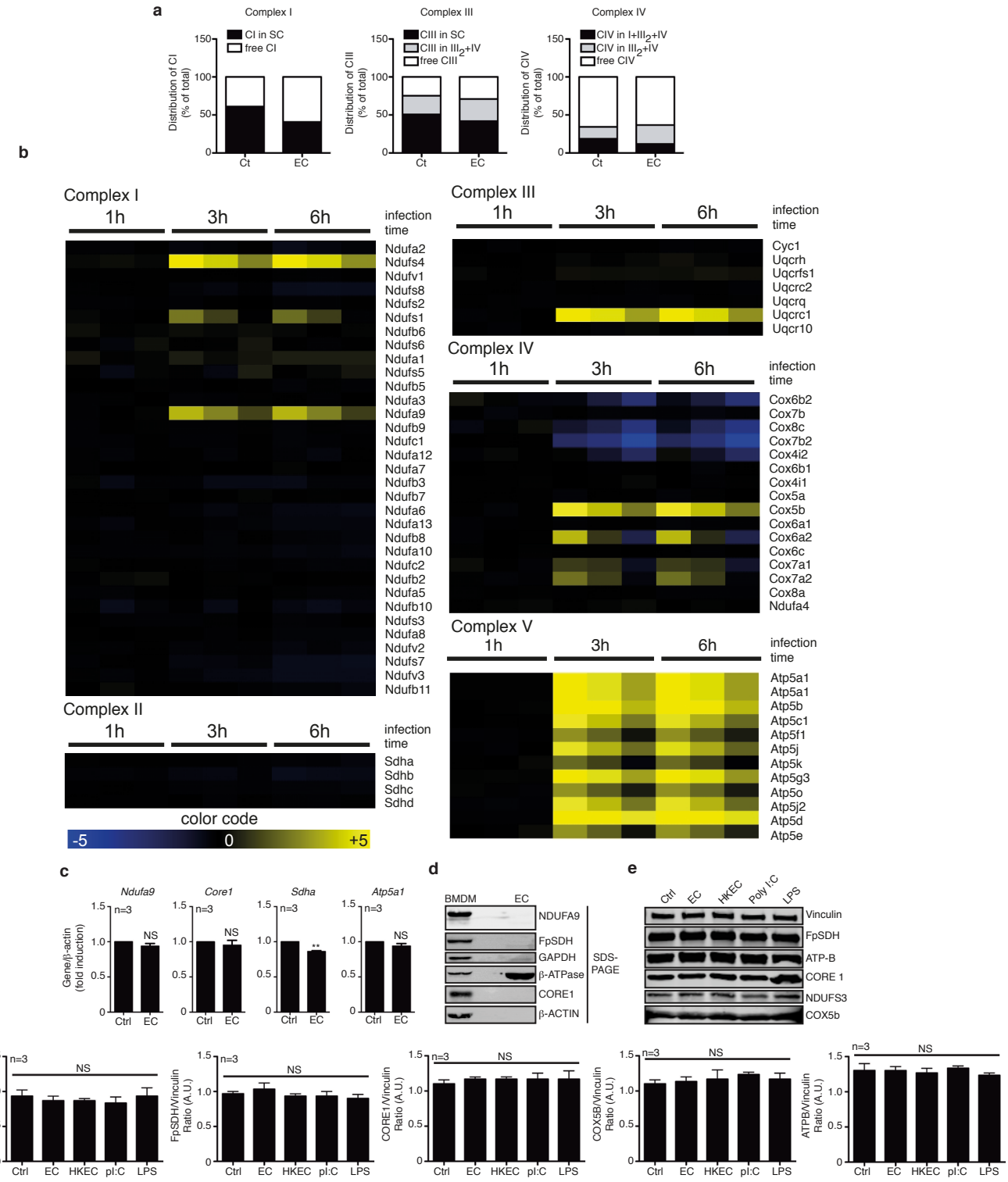

Supplementary Figure 1 Effect of *E. coli* challenge on mitochondrial respiratory complex subunit expression in BMDMs. (**a**) Densitometric analysis of the distribution of complex I, III and IV as determined from Figure 1a. (**b**) Gene microarray analysis (Affymetrix Microarray data have been previously deposited with the NCBI Gene Expression Omnibus under accession number GSE27960 by Sander L.E. et al., see ref. 8) of *C57BL/6J* BMDMs treated with *E. coli* for 1, 3 or 6h (3 biological replicates). A heat map of nuclear genome-encoded mitochondrial respiratory complexes subunits is shown. (**c**) Q-PCR analysis of the indicated gene from BMDMs treated with *E. coli* for 1.5h. N=3. (**d**) Immunoblot analysis of resting BMDMs and *E. coli*. (**e**) Immunoblot analysis of BMDMs treated as indicated for 1.5h. EC, *E. coli* ; HKEC, heat killed-*E. coli* ; Poly I:C, polyinosinic:polycytidylic acid ; LPS, lipopolysaccharide. (**f**) Quantification analysis of SDS-PAGE as in (**e**). n=3. In (**d**) and (**e**), membranes were probed with the indicated antibodies specific for components of the ETC. Data presented are mean +/- s.e.m. of 3 independent experiments (**c, f**). NS, not significant; **P < 0.01 by two-tailed unpaired t-test.

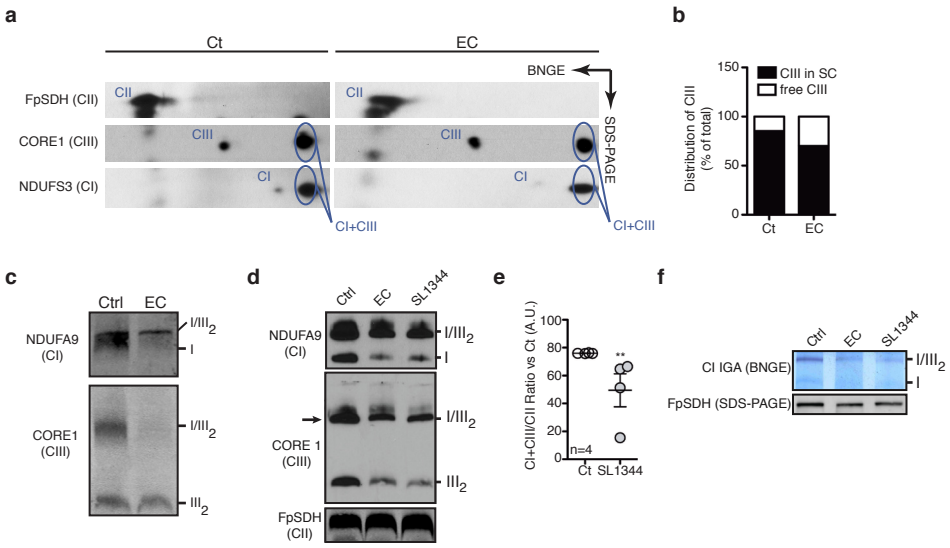

Supplementary Figure 2 Detection of Gram-negative bacteria induces ETC rearrangement and is associated with decreased complex I. (**a**) Immunoblot of a bi-dimensional gel analysis (First dimension: BN-PAGE, second dimension: SDS-PAGE) of mitochondria isolated from *C57BL/6J* BMDMs treated or not with EC for 1.5h. (**b**) Quantification from (**a**) of the proportion of free CIII and CIII in super-complex with CI (SC I+III). (**c**) BN-PAGE immunoblot of thioglycollate-elicited *C57BL/6J* macrophages treated or not with EC. (**d**) BN-PAGE immunoblot of *C57BL/6J* BMDMs treated with *E. coli* and *S. enterica* Typhimurium for 1.5h. (**e**) Densitometric analysis of BN-PAGE from (**d**) showing CI+CIII SC proportion *vs*. CII. **P < 0.01 by two-tailed unpaired t-test. Data present mean +/- s.e.m. of 4 independent experiments. (**f**) CI IGA of BMDMs treated or not with *E. coli* or *S. enterica* Typhimurium for 1.5h. SDS-PAGE analysis of FpSDH (CII) is shown (lower panel).

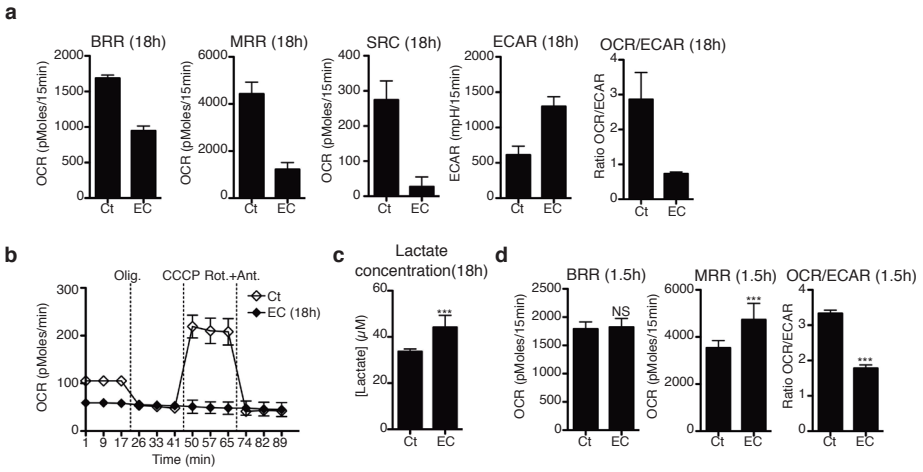

Supplementary Figure 3 *E. coli* challenge influences mitochondrial respiration and glycolysis in macrophages. (**a**) Glucose-driven basal respiration rate (BRR), maximum respiration rate (MRR), spare respiration capacity (SRC), basal extracellular acidification rate (ECAR) and oxygen consumption rate (OCR)/ECAR ratio in BMDMs treated or not with EC for 18h. Data present means +/- S.D. of one representative of 3 independent experiments. (**b**) Glucose-driven OCR upon sequential treatment of oligomycin (olig.), CCCP, and rotenone+antimycin (Rot.+Ant.) of BMDMs treated or not with EC for 18h. Data present means +/- S.D. of one representative of 3 independent experiments (**c**) Extracellular lactate release by BMDMs treated or not with EC for 18h. (**d**) Glucose-driven BRR, MRR and OCR/ECAR ratio of BMDMs treated or not with EC for 1.5h. Error bars, s.e.m. NS, not significant, ***P < 0.001 by two-tailed unpaired t-test. Data in (**c, d**) present mean +/- s.e.m. of 3 independent experiments performed in 4 to 6 replicates.

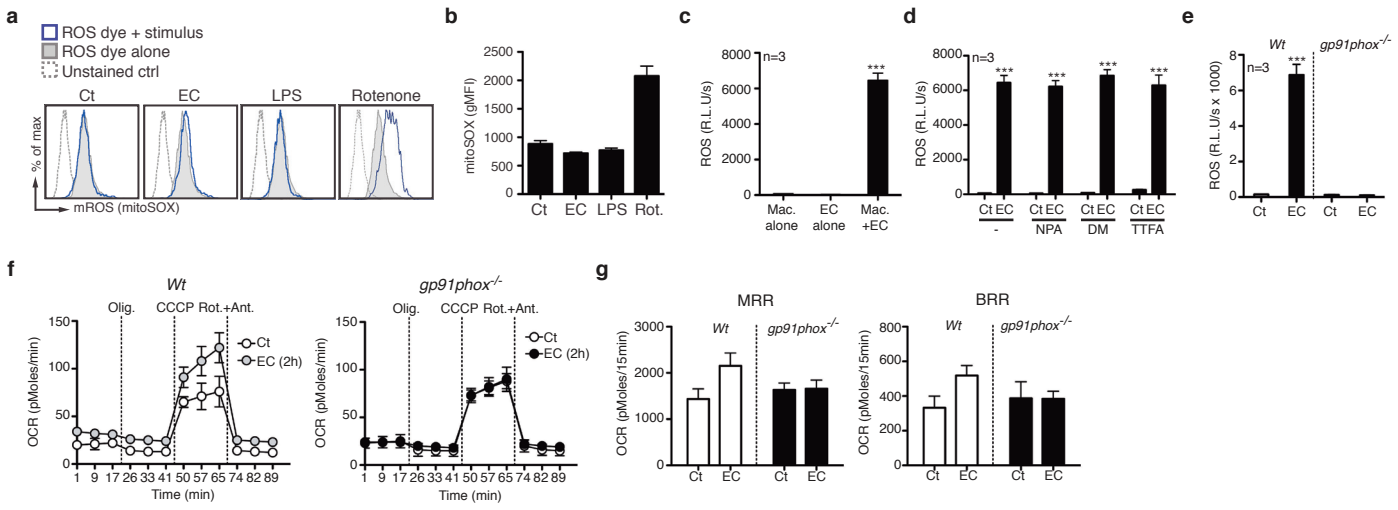

Supplementary Figure 4 Bacteria recognition drives mitochondrial respiratory adaptations through phagosomal NADPH oxidase-mediated ROS. (**a**) Representative histograms of BMDMs treated as indicated for 1.5h, stained with mitoSOX (mROS) and analysed by FACS. Rot., rotenone. (**b**) mROS production by BMDMs treated as in (**a**). One representative experiment performed in triplicate is shown. Data are mean +/- S.D. (**c-e**) ROS production by EC alone (**c**), Wt BMDMs (**c-e**) and *gp91phox-/-* BMDMs stimulated or not with EC for 15min (**e**). ROS production was monitored by chemiluminescence and expressed as relative light units per second (R.L.U./s). In (**d**), BMDMs were treated with the CII inhibitors 3-nitropropionic acid (NPA), dimethyl-malonate (DM) or thenoyltrifluoroacetone (TTFA). (**f**) Glucose-driven OCR upon sequential treatment of oligomycin (olig.), CCCP, and rotenone+antimycin (Rot.+Ant.) of *Wt* and *gp91phox-/-* BMDMs challenged with EC for 2h. (**g**) Maximum (MRR) and basal (BRR) respiration rate of *Wt* and *gp91phox-/-* BMDMs challenged with EC for 2h. one representative experiment is shown. NS, not significant; **P<0.01 by unpaired t-test analysis. Data present mean +/- s.e.m. of 3 to 4 independent experiments performed in duplicates (**c-e**). Data present mean +/- S.D. of one representative of 3 independent experiments performed in 4-6 replicates (**f, g**). *P < 0.05; ***P < 0.001 by two-tailed unpaired t-test.

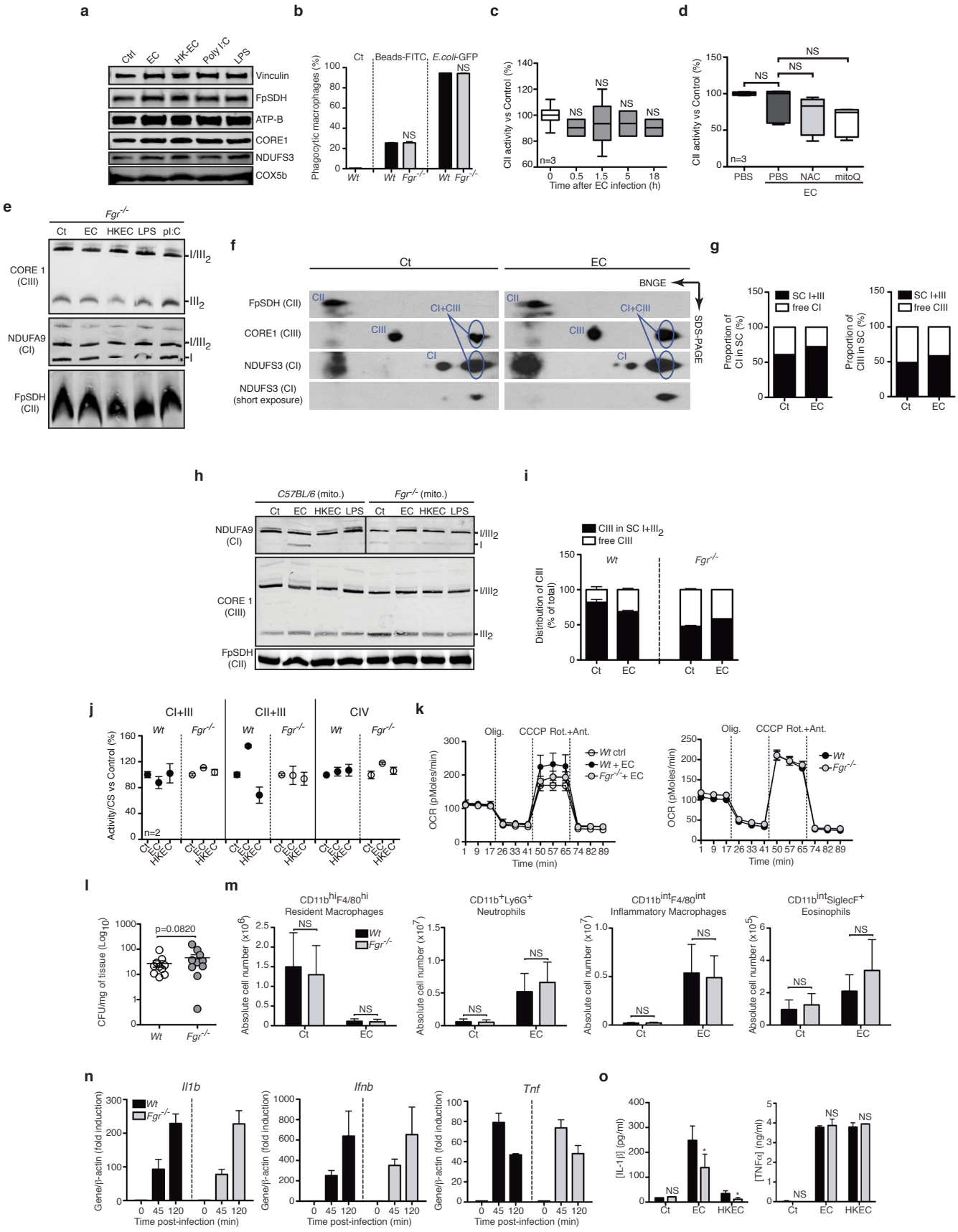
a
Ctrl
EC
HK-EC
Poly I:C
LPS
Vinculin
FpSDH
ATP-B
CORE1
NDUFS3
COX5b
b
Ct
Beads-FITC
E.coli-GFP
Phagocytic macrophages (%)
NS
Wt
Fgr-/-
c
CII activity vs Control (%)
n=3
Time after EC infection (h)
d
CII activity vs Control (%)
PBS
NAC
mitoQ
EC
e
Fgr-/-
Ct
EC
HKEC
LPS
pI:C
CORE 1 (CIII)
NDUFA9 (CI)
FpSDH (CII)
f
Ct
EC
BNGE
SDS-PAGE
FpSDH (CII)
CORE1 (CIII)
NDUFS3 (CI)
NDUFS3 (CI) (short exposure)
CII
CI+CIII
CIII
CI
g
SC I+III
free CI
free CIII
Proportion of CI in SC (%)
Proportion of CIII in SC (%)
h
C57BL/6 (mito.)
Fgr-/- (mito.)
NDUFA9 (CI)
CORE 1 (CIII)
FpSDH (CII)
i
CIII in SC I+III2
free CIII
Distribution of CIII (% of total)
j
CI+III
CII+III
CIV
Activity/CS vs Control (%)
n=2
k
Olig.
CCCP
Rot.+Ant.
Wt ctrl
Wt + EC
Fgr-/- + EC
OCR (pMoles/min)
Time (min)
l
CFU/mg of tissue (Log10)
p=0.0820
m
CD11bhiF4/80hi Resident Macrophages
CD11b+Ly6G+ Neutrophils
CD11bintF4/80int Inflammatory Macrophages
CD11bintSiglecF+ Eosinophils
Absolute cell number
n
Il1b
Ifnb
Tnf
Gene/β-actin (fold induction)
Time post-infection (min)
o
[IL-1β] (pg/ml)
[TNFα] (ng/ml)

Supplementary Figure 5 Fgr deficiency prevents macrophage ETC adaptations and attenuates innate immunity in response to *E. coli* detection. (**a**) Immunoblot analysis of BMDMs stimulated as indicated for 1.5h and probed with the indicated antibodies specific for component of the ETC. (**b**) Percentage of phagocytic cells of *Wt* and *Fgr*$^{-/-}$ BMDMs treated with NPA and cultured with GFP-expressing *E. coli* (*E. coli*-GFP) or FITC-labeled latex beads (Beads-FITC) for 20min. (**c, d**) Spectrophotometric CII activity in permeabilized *Fgr*$^{-/-}$ BMDMs stimulated with EC for 1.5h or the indicated time points and treated or not with with N-acetylcystein (NAC) or mitoQ. (**e**) Immunoblot of BN-PAGE analysis of permeabilized *Fgr*$^{-/-}$ BMDMs stimulated as indicated for 1.5h. (**f**) Immunoblot of a bi-dimensional gel analysis (BN-PAGE followed by a SDS-PAGE) of mitochondrial isolated from *Fgr*$^{-/-}$ BMDMs treated or not with *Escherichia coli* (EC) for 1.5h. (**g**) Quantification from (**f**) of the proportion of CI and CIII as free form or in super-complex (SC I+III). (**h**) Immunoblot of BN-PAGE analysis of mitochondrial isolated from *Wt* and *Fgr*$^{-/-}$ BMDMs stimulated as indicated for 1.5h. Lower panel shows CI in-gel activity (IGA). (**i**) Relative contribution of CIII to SC as determined by BN-PAGE analysis of mitochondria isolated from *Fgr*$^{-/-}$ and *Wt* BMDMs. Quantification from 2 separate gels from the same experiment is shown. Data are means +/- S.D. (**j**) Effect of *E. coli*-stimulation on the indicated ETC complex activities in mitochondria isolated from *Wt* and *Fgr*$^{-/-}$ BMDMs. (**k**) Glucose-driven OCR upon sequential treatment of oligomycin (olig.), CCCP, and rotenone+antimycin (Rot.+Ant.) of *Wt* and *Fgr*$^{-/-}$ BMDMs stimulated or not with EC for 2h. (**l**) Splenic bacterial burdens 72h after injection of 1 x 10^8 of viable *E. coli* into the peritoneal cavity of *Wt* and *Fgr*$^{-/-}$ mice. Each symbol represents one mouse. (**m**) Absolute cell numbers determined at 18h by FACS of the indicated cell populations in the peritoneal cavity of *Wt* and *Fgr*$^{-/-}$ mice injected with 1x10^8 viable EC (n=3 to 5 per group). (**n**) mRNA levels in *Wt* and *Fgr*$^{-/-}$ BMDMs stimulated with EC for the indicated time point (n=3). (**o**) Cytokine levels in supernatants of *Wt* and *Fgr*$^{-/-}$ BMDMs stimulated with EC for 18h. Error bars, s.e.m. NS, not significant; *P < 0.05, ***P<0.001 by two-tailed unpaired t-test. Data present mean +/- s.e.m. of 2 to 4 independent experiments performed in 2 to 6 replicates (**b-d, j, l-o**). Data in (**k**) are means +/- s.d. of 4 to 5 technical replicates from one representative of at least 3 independent experiments. EC, *E. coli* ; HKEC, heat killed-*E. coli* ; pI:C, polyinosinic:polycytidylic acid ; LPS, lipopolysaccharide.

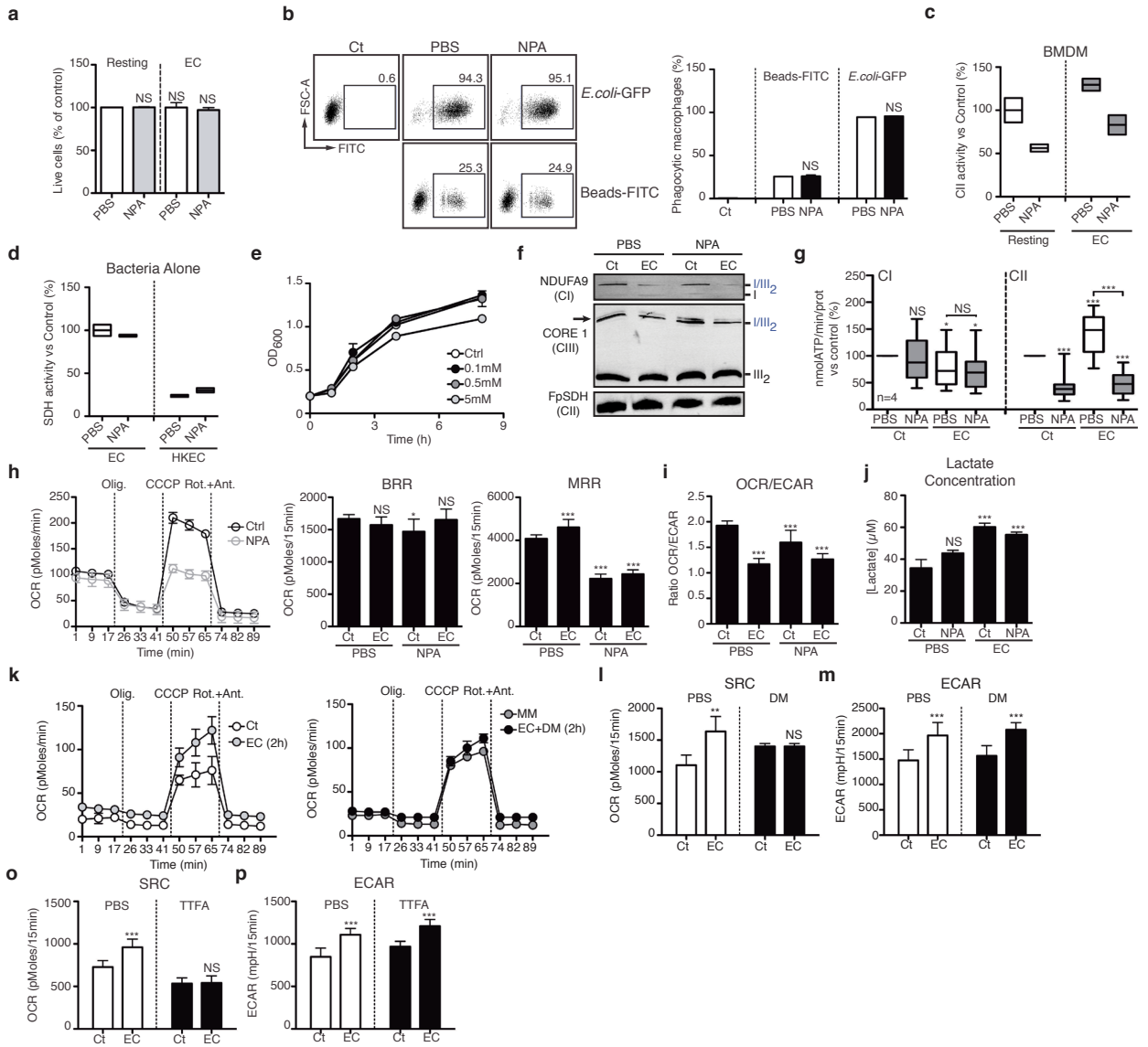

Supplementary Figure 6 Effects of mitochondrial complex II (CII) inhibition on BMDM functions and mitochondrial respiration. (**a**) Percentage of live BMDMs treated with 0.5mM NPA and challenged with EC for 1.5h. Cells were stained with annexin-V-GFP and 7-aminoactinomycin D (7-AAD) and analyzed by fluorescent-activated cell sorting flow cytometry (FACS). Live cells were defined as annexin-V-/7-AAD- cells. (**b**) Percentage of phagocytic cells (right panel ; n=3) of BMDMs treated with 0.5mM NPA and cultured with GFP-expressing *E. coli* (*E. coli*-GFP) or FITC-labeled latex beads (Beads-FITC) for 20min. Representative FACS plots (left panel) are shown. (**c**) Spectrophotometric CII activity of BMDMs treated or not with EC in presence of 0.5mM NPA. One representative experiment is shown. (**d**) Spectrophotometric SDH activity of log phase EC or heat-killed EC (HKEC) in the presence of NPA. (**e**) *E. coli* growth measured by spectrophotometry (OD_{600}) in presence of the indicated concentrations of NPA over a course of 8h (n=3). (**f**) BN-PAGE immunoblot or permeabilized *C57BL/6J* BMDMs treated or not with NPA stimulated with EC for 1.5h. Membranes were stained with the indicated antibodies. (**g**) Glutamate+malate (CI) or succinate (CII)-driven ATP synthesis activity in permeabilized *C57BL/6J* BMDMs treated or not with NPA stimulated with EC for 1.5h. (**h**) Glucose-driven OCR, BRR and MRR upon sequential treatment of oligomycin (olig.), CCCP, and rotenone+antimycin (Rot.+Ant.) of BMDMs treated or not with NPA and challenged with EC for 2h. (**i**) OCR/ECAR ratio of BMDMs treated or not with NPA and challenged with EC for 2h. (**j**) Lactate production by BMDMs treated or not with NPA and challenged with EC for 2h. (**k**) Glucose-driven OCR, BRR and MRR upon sequential treatment of oligomycin (olig.), CCCP, and rotenone+antimycin (Rot.+Ant.) of BMDMs treated or not dimethyl-malonate (DM) and challenged with EC for 2h. (**l-p**) SRC and ECAR of BMDMs treated or not with dimethyl-malonate (DM) or thenoyltrifluoroacetone (TTFA) and challenged with EC for 2h. Error bars, s.e.m. NS, not statistically significant; *P < 0.05; ***P < 0.001 by two-tailed unpaired t-test. Data present mean +/- s.e.m. of 2 to 4 independent experiments performed in 2- to 6 replicates (**a, b, e, g, i, j, l-p**). Data in (**c, d, h, k**) are means +/- s.d. of 3 technical replicates from one representative of at least 3 independent experiments.

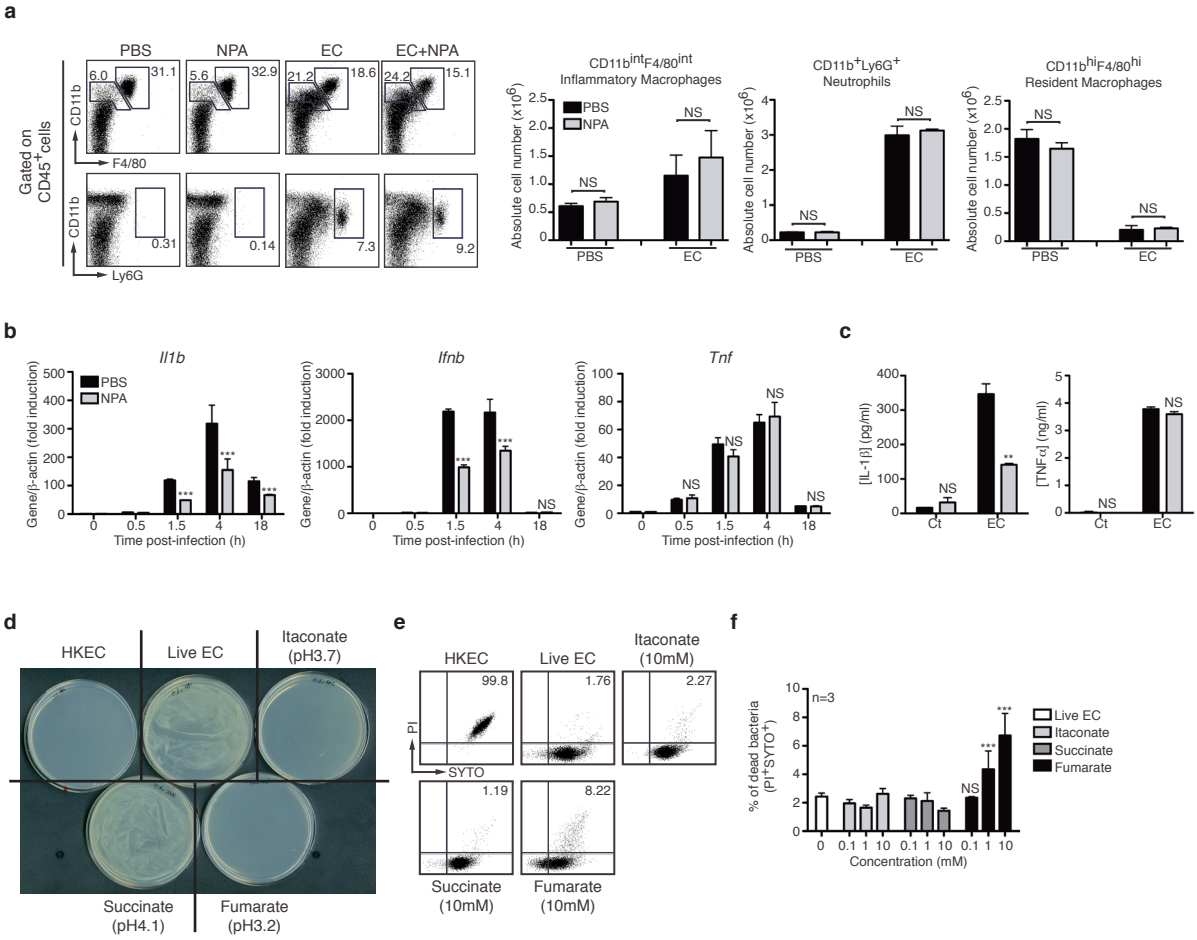

Supplementary Figure 7 Complex II activity is required for macrophage bactericidal functionand CII inhibition by 3-nitropropionic acid (NPA) alters innate immune response to viable *E. coli*. (**a**) Absolute cell numbers at 18h (right panels) of the indicated cell populations in the peritoneal cavity of *C57BL/6J* mice treated or not with 50mg/kg NPA and injected with $1x10^8$ viable EC (n=3 to 5 per group). Representative FACS plots (left panels) are shown. (**b, c**) mRNA (**b**) and cytokine levels (**c**) in BMDMs treated or not with NPA and stimulated with EC for the indicated time points (n=3). (**d**) Representative photographs of Petri dishes containing bacteria grown overnight after treatment with the indicated chemicals for 6h. As control, heat-killed *E. coli* (HKEC) were plated. (**e**) Representative flow cytometry plots of *E.coli* treated with the indicated reagents for 6h. (**f**) Percentage of PI+SYTO+ bacteria after 6h treatment with increasing amount of the indicated reagents. N=3. Error bars, s.e.m. NS, not significant; **P < 0.01 ***P < 0.001 by two-tailed unpaired t-test. Data (**a,b,c,f**) present mean +/- s.e.m. of 2 to 3 independent experiments performed in 2- to 6 replicates.

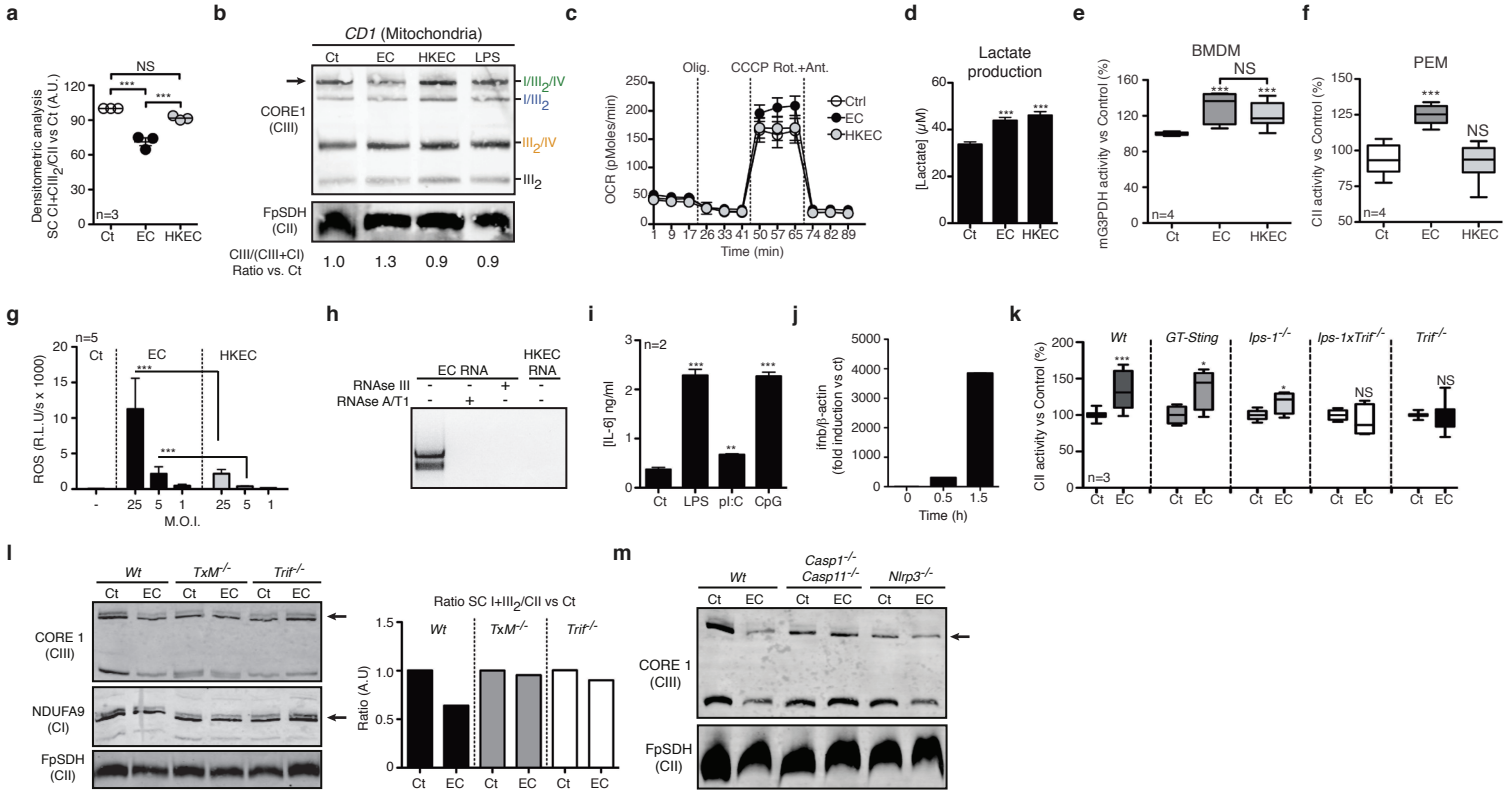

Supplementary Figure 8 Bacteria viability-specific ETC adaptations involves both TLR signaling and the Nlrp3 inflammasome. (**a**) Densitometry analysis of CI+$CIII_2$/CII signal ratio as observed by BNGE immunoblot of *C57BL/6J* BMDMs stimulated or not with EC and HKEC for 1.5h (n=3). Error bars, s.e.m. NS, not significant; ***P < 0.001 by one-way ANOVA followed by Tukey post-test analysis. (**b**) Blue-native gel electrophoresis (BN-PAGE) immunoblot in mitochondria isolated from *CD1* BMDMs stimulated with EC, HKEC or lipopolysaccharide (LPS) for 1.5h. (**c**) Glucose-driven OCR upon sequential treatment of oligomycin (olig.), CCCP, and rotenone+antimycin (Rot.+Ant.) of BMDMs treated or not with viable *E. coli* EC or heat-killed *E. coli* (HKEC) for 2h. (**d**) Lactate production by BMDMs treated with EC or HKEC for 2h. (**e**) Spectrophotometric G3PDH activity in BMDM stimulated with viable EC or HKEC for 1.5h. (**f**) Spectrophotometric CII activity in permeabilized thioglycollate-elicited peritoneal macrophages (PEM) stimulated with viable EC or HKEC for 1h. (**g**) ROS production by *Wt* BMDMs stimulated with EC or HKEC at the indicated multiplicity of infection (M.O.I.) for 15min. ROS production was monitored by chemiluminescence and expressed as relative light units per second (R.L.U./s). (**h**) Agarose gel electrophoresis of EC and HKEC total RNA before and after treatment with RNases III and A/T1. (**i**) IL-6 cytokine levels in supernatants of *Wt* BMDMs treated with the indicated TLR ligand (n=2). **j,** Ifnb mRNA levels in *Wt* BMDMs stimulated with poly(I:C) for the indicated time point. (**k**) Spectrophotometric CII activity in permeabilized *Wt*, *Trif*$^{-/-}$, *Ips*$^{-/-}$, *Trif*$^{-/-}$x*Ips*$^{-/-}$ and *Sting* deficient (*GT-Sting*) BMDMs stimulated with viable *E. coli* (EC) for 1.5h. (**l**) BNGE analysis from permeabilized *Wt*, *Trif*$^{-/-}$, and *Trif*$^{-/-}$x*Myd88*$^{-/-}$ (*TxM*$^{-/-}$) BMDMs stimulated with EC for 1.5h. Arrows indicate the main SCs affected. Densitometry analysis of the SCI+III_2 vs CII is shown on the right panel. (**m**) Representative BNGE analysis from permeabilized *Wt*, *Caspase1*$^{-/-}$x*Caspase11*$^{-/-}$ (*Casp1*$^{-/-}$x*Casp11*$^{-/-}$) and *Nlrp3*$^{-/-}$ BMDMs stimulated with EC for 1.5h. Arrows indicate the main SCs affected. NS, not significant; *P < 0.05; ***P < 0.001 by two-tailed unpaired t-test. Data present mean +/- s.e.m. of 3 to 4 independent experiments performed in duplicates (**a, d, e, f, g, i**). Data in (**c**) present mean +/- S.D. of one representative experiment performed in 6 technical replicates.